Preparation and Characterization of Magnesia-based Powder Added With Transition Metal

Bong-Gu Kim
Changwon National University
Hyun-Hee Choi
Changwon National University
Jung-Hun Son
Changwon National University
SeungCheol Yang
Changwon National University
Min-Seok Kwon
POSCO Research Institute
Asimiyu A. Tiamiyu
IUPUI: Indiana University Purdue University at Indianapolis
Jing Zhang
IUPUI: Indiana University Purdue University at Indianapolis
Yeon-Gil Jung (jungyg@changwon.ac.kr)
School of Nano & Advanced Materials Engineering, Changwon National University, 20 Changwondaehak-ro, Changwon, Gyeongnam 51140, Republic of Korea

Research Article

Keywords: Magnesia, Coprecipitation, Substitutional element, Binary composition powder, Reactivity

Posted Date: November 3rd, 2020

DOI: https://doi.org/10.21203/rs.3.rs-99562/v1

Preparation and Characterization of Magnesia-Based Powder Added with Transition Metal

Bong-Gu Kim[1], Hyun-Hee Choi[1], Jung-Hun Son[1], SeungCheol Yang[1], Min-Seok Kwon[2] ,

Asimiyu A. Tiamiyu[3], Jing Zhang[3], Yeon Gill Jung[1,*]

[1]School of Nano & Advanced Materials Engineering, Changwon National University,
20 Changwondaehak-ro, Changwon, Gyeongnam 51140, Republic of Korea

[2]Steelmaking Research Group, Technical Research Laboratories, POSCO1,

Goedong-dong, Nam-gu, Pohang-shi, Gyeongbuk

[3] Department of Mechanical Engineering, Indiana University-Purdue University Indianapolis,,

723 West Michigan Street, Indianapolis, IN 46202

[*]Corresponding author

E-mail address: jungyg@changwon.ac.kr (Y.G.Jung)

ABSTRACT

The solid-phase reaction method for preparing forsterite (Mg_2SiO_4) using MgO and SiO_2 powders has the disadvantages of high reaction temperature, long reaction time, and inhomogeneous reaction depending on the particle size of MgO. Therefore, MgO-based powders with a high reactivity were synthesized using a coprecipitation method with substitutional elements (Mn or Ni), and the effects of processing parameters on synthesizing MgO-based binary composition powders were investigated through the particle characteristics. The crystal structure continuously changed with the contents of the substitutional element, showing the same trend as the atomistic simulation results. The MgO-based powders showed higher reactivity than the conventional MgO powder, which could be confirmed in the particle characteristics, such as particle size and crystallinity, obtained in a short reaction time, and at a relatively low temperature. The optimum composition ratio in the binary composition powder for forming the Mg_2SiO_4 depended on the type of substitutional element, and the reaction mechanism was identified based on the particle characteristics.

Keywords:

Magnesia

Coprecipitation

Substitutional element

Binary composition powder

Reactivity

1. Introduction

Ceramic powders are synthesized using various methods, such as solid state reaction, sol–gel reaction, hydrothermal synthesis, and coprecipitation [1–4]. The solid state reaction method is the most widely used for producing polycrystalline ceramic powders from mixtures of solid starting materials [5,6]. There is no waste disposal problem in the solid state reaction method because there is no need for solvent in the reaction [5], while there is a disadvantage of expensive construction and its maintenance because it should be conducted at a high temperature of 1000–1500 °C [6]. In addition, this process requires a long reaction time, and the uniformity in the reaction depends on the particle size and distribution [7].

Forsterite (Mg_2SiO_4) is employed as an insulator in tubes, substrate for resistors, substrate for integrated circuits, and an implant material, owing to its excellent properties, such as excellent insulation performance, low dielectric loss, high mechanical strength, excellent thermal stability, and large coefficient of thermal expansion [7–10]. Therefore, the various synthetic methods mentioned above have been studied for the successful synthesis of Mg_2SiO_4 [7–16]. Among these methods, the solid state reaction from mixtures of magnesia (MgO) and silica (SiO_2) powders has been generally utilized for the simple synthesis of Mg_2SiO_4 without post-solvent and environmental problems. However, the solid state reaction between powders requires a high temperature of over 1500 °C and longer reaction time during the reaction compared with other methods [1,5,6]. To improve the issues of high process temperature and long reaction time in the solid state reaction for preparing Mg_2SiO_4, various studies have been undertaken to increase the reactivity of MgO and SiO_2 powders [12–16]. Ta-Wui Cheng et al. reported that the reaction temperature in the solid state method could be reduced to 1500 °C by adding serpentine [12]. Lin Cheng et al. increased the surface activity by employing nanosized MgO and SiO_2 powders prepared using a high-energy milling method, and reduced the heat-treatment temperature to 850 °C [13]. Liugang Chen et

al. synthesized Mg_2SiO_4 at 850 °C using MgO precursors such as magnesium hydroxide ($Mg(OH)_2$) or magnesium carbonate ($MgCO_3$) [15,16].

MgO, which can be utilized for synthesizing Mg_2SiO_4 by the solid state reaction, has been prepared by several methods, such as coprecipitation, electrodeposition, sol–gel technique, hydrothermal, solvothermal, preparation using a bubbling setup, and microwave-assisted synthesis [17]. Among the various methods, the coprecipitation technique is a simple and cost-effective method to produce ceramic powder, including MgO, by adding a chemical precipitant to a cation-containing solution or by changing temperature and/or pressure. It is possible to synthesize powder under various conditions by adjusting the concentration, pH, mixing and stirring speed, and solution temperature [18–21]. In addition, coprecipitation can be an efficient manufacturing procedure to produce MgO-based binary powders with uniform properties across their surface, thereby controlling the physical and chemical properties of MgO-based binary powders and assisting the determination of the structure–activity relationships [22].

The three oxides, MgO, nickel oxide (NiO), and manganese oxide (MnO), play similar roles in minerals because the cations have the same charge and similar radii. Each combines to form an olivine structure (structure of Mg_2SiO_4), and undoubtedly there is complete miscibility between these three olivine members at high temperatures [23,24]. NiO and MnO are of particular interest in the solid solution research on MgO, having the same rock salt crystal structure as MgO, and all three compounds have approximately the same unit cell dimensions [25], confirming that the addition of MnO and NiO to MgO lowers the melting point of the solid solution and tends to decrease in temperature as the addition amount increases. Based on this concept, it is necessary to develop a new composition and/or a new MgO-based powder for preparing Mg_2SiO_4 at a lower temperature with a short reaction time and a uniform reactivity.

Therefore, in this study, new MgO-based binary composition powders were prepared using the coprecipitation method, in which it is easy to control the various parameters mentioned above. The Ni and Mn as substitutional elements were employed to prepare the binary powders. The reactivity of MgO and binary powders with SiO_2 was compared in preparing Mg_2SiO_4 through particle characteristics. The optimal composition ratio in the binary powders was induced with the type of substitutional element, and its reaction mechanism for forming Mg_2SiO_4 was proposed and discussed based on the particle characteristics, such as particle size and crystallinity.

2. Material and methods

2.1. Preparation of MgO-based binary powder

Magnesium chloride ($MgCl_2$; Yakuri Pure Chemicals Co., Ltd., Kyoto, Japan), nickel chloride ($NiCl_2$; Daejung Chemicals & Metals Co., Ltd., Shiheung, Republic of Korea), and manganese chloride ($MnCl_2$: Sigma-Aldrich Korea, Yong-in, Republic of Korea) were used as starting materials, in which the $NiCl_2$ and $MnCl_2$ were employed as precursors of substitutional elements. Sodium hydroxide (NaOH; Daejung Chemicals & Metals Co., Ltd.) was used as a reaction catalyst. Each starting material was dissolved in distilled water to 0.5 M concentration and then mixed with mole ratios as shown in Table 1. In this study, two binary powders of $Mg_{1-x}Ni_xO$ and $Mg_{1-x}Mn_xO$ were prepared with the composition ratios shown in Table 1.

In addition, the single-composition powders of MgO, NiO, and MnO were synthesized as reference powders. Each precursor solution was mixed by stirring at 300 rpm for 30 min at room temperature, and then the pH of each mixed solution was adjusted to 9, 11, and 13 by dropwise addition of NaOH. In addition, the pH was fixed at 11 with controlling the concentration of NaOH as 0.1, 0.5, and 1 M to investigate the effect of catalytic concentration

on the nuclei growth rate. Again, stirring at 300 rpm for 1 h was conducted for uniform dispersion of each metal hydroxide converted from each metal chloride (each precursor). The reacted and precipitated powder was washed five times with distilled water, dried at 100 °C for 24 h, and then ground. Each powder was heat-treated at 600, 800, 1000, and 1200 °C in an inert atmosphere for the Mg–Ni binary powder and in a reducing atmosphere for the Mg–Mn binary powder [26]. To investigate the effects of the pH value and the concentration of catalyst on the particle size and morphology, the heat treatment was conducted using a specified composition of $Mg_{0.7}M_{0.3}O$ (M = Ni and Mn) at 1200 °C in an inert atmosphere for the Mg–Ni binary powder and in a reducing atmosphere for Mg–Mn binary powder. The detailed process for preparing the MgO-based binary powders is illustrated in Fig. 1.

In addition, to evaluate the reactivity of the synthesized powder with SiO_2, the pellet-type sample was prepared by mixing each powder (MgO, Mg–Ni binary powder, Mg–Mn binary powder) and SiO_2 with a mole ratio of 2:1, followed by ball milling for 24 h, and then heat treatment was performed at 1200 °C in a reducing atmosphere. The heat-treatment atmosphere for the reactivity test was decided based on a real application condition. The MgO-based powders for the reactivity test were prepared at 800 °C in an inert atmosphere for the Mg–Ni binary powder and in a reducing atmosphere for the Mg–Mn binary powder, while the MgO powder heat-treated in the inert atmosphere was employed in the reactivity test.

2.2. Characterization

The phase analysis for the synthesized MgO-based binary powders and the Mg_2SiO_4 samples obtained from the reactivity test were characterized using X-ray diffraction (XRD; MiniFlex II; Rigaku, Tokyo, Japan) with Cu Kα radiation (λ = 1.54060 Å) in the 2θ range from 20° to 80° with a scan speed of 2°/min. The average crystallite size (D) was calculated from the full width at half maximum (FWHM) of the XRD peak using the Scherrer equation

[27]:

$$D = \frac{K\lambda}{B\cos\theta},$$

where K is a constant (0.94), λ is the wavelength of the X-rays (0.15406 nm), B is the FWHM of a diffraction peak, and θ is the diffraction angle. The morphology and size of the synthesized powders were investigated using a field emission scanning electron microscope (FE-SEM; CZ/MIRAI LMH/H.S. Code: 9012.10.1000; TESCAN, Brno, Czech). The cross-sectional microstructure of Mg_2SiO_4 samples was observed using an SEM (JSM-5610; JEOL, Japan) and its chemical composition was identified using an energy-dispersive spectrometer (EDS; Oxford Instruments, UK) attached to the SEM.

2.3 Atomistic simulation for crystal structural property in MgO-based powder

Two types of atomistic simulations were conducted. The first is a molecular dynamics (MD) model to simulate Young's modulus of MgO and doped MgO (*i.e.*, $Mg_{1-x}Ni_xO$ and $Mg_{1-x}Mn_xO$, where x = 0.03, 0.06, and 0.12) using a simulated tensile test. The MD model uses the pairwise potential with partial charges proposed by Pedone et al. [28] and is implemented with customized codes in the LAMMPS MD simulation package [29]. This potential includes a Morse potential with an additional repulsive term and long-range Coulomb interaction. Compared with the commonly used BKS potential, a pairwise potential has the advantage of more stable convergence at a wide range of temperature.

The second atomistic model is to simulate the phases in XRD using Materials Studio's Reflex module. The calculation is based on models of crystalline materials of MgO and doped MgO. A 2 × 2 × 2 supercell structure of MgO was geometrically optimized. The XRD spectrum of pure MgO was calculated. Then, compositions of 1.5, 3, 6, and 12% for each doping element (Mn or Ni) were compared with one another to establish the phase-shift

relationship in crystal structures, and the theoretical and experimental results were compared.

3. Results and discussion

3.1. Powder characteristics with the species and content of the substitutional element

The XRD patterns of the $Mg_{1-x}Ni_xO$ (x = 0–1) powders synthesized at pH 11 are shown in Fig. 2 before and after heat treatment in an inert atmosphere (Ar atmosphere). As the temperature increased, the width of the peak narrowed, indicating that the phase was stable [27,30]. As the amount of Ni in the $Mg_{1-x}Ni_xO$ composition was increased, the peak was slightly shifted to a higher angle. The peak should be shifted according to Bragg's law [31,32] because the ion radius of Ni (69 pm) is smaller than that of Mg (72 pm). Through this result, it was confirmed that the Mg–Ni binary powder was completely synthesized as a solid solution until the composition of $Mg_{0.5}Ni_{0.5}O$. Therefore, the $Mg_{0.7}Ni_{0.3}O$ powder with an intermediate composition was used for investigating the particle size and morphology.

Fig. 3 shows the particle size and morphology of the MgO, $Mg_{0.7}Ni_{0.3}O$, and NiO powders synthesized at each temperature. The particle size in all powders increased with increasing temperature, showing a bigger particle size in the NiO powder, while the particle size of $Mg_{0.7}Ni_{0.3}O$ powder did not grown much with the temperature, compared with those of the MgO and NiO powders. In particular, the particle size of MgO powder was too small at 600 °C, which was employed as the reference powder. The particle morphology of the MgO, $Mg_{0.7}Ni_{0.3}O$, and NiO particles became polygonal at 1000, 1200, and 800 °C, respectively. Based on the XRD analysis and particle size observation, the most suitable heat-treatment temperature was considered to be 800 °C for preparing the Mg–Ni-based binary powder, showing a similar particle size of 0.09 ± 0.04 μm and crystallinity with the MgO powder of 0.08 ± 0.04 μm.

The XRD patterns of the $Mg_{1-x}Mn_xO$ (x = 0–1) powders synthesized at pH 11 are shown in Fig. 4 before and after heat treatment in a reducing atmosphere of 95%Ar–5%H_2. Because $Mn(OH)_2$ forms Mn_3O_4 during the drying process in an ambient atmosphere, the OH^- should be removed during the heat treatment for synthesizing the Mg–Mn binary and MnO powders [32]. In the Mg–Mn binary system, the XRD peak was shifted to a lower angle with increasing Mn content because the ionic radius of the Mn(II) (83 pm) ion is larger than that of the Mg ion, according to Bragg's law [33,34]. When the amount of Mn in the $Mg_{1-x}Mn_xO$ composition was increased, an amorphous phase was detected in the as-synthesized powders as shown in Fig. 4(A). This phenomenon was also observed at a relatively low temperature of 600 °C (Fig. 4(B)). The difference in the ionic radius between Mg and Mn is larger than that between Mg and Ni, showing a certain peak shift and a phase transition from $Mg(OH)_2$ to Mn_3O_4 with increasing Mn content, even though the following Hume-Rothery rules are satisfied—The ionic radii of Mn and Mg ions are within 15%, showing the same structure (rock salt), valence, and electronegativity [33]. On increasing the temperature, the crystallinity was enhanced and the solid solution was formed with a single phase. Finally, the Mg–Mn binary powders were completely synthesized in all compositions of Table 1 at 1000 °C, even in the reducing atmosphere.

The particle size and morphology of the MgO, $Mg_{0.7}Mn_{0.3}O$, and MnO powders synthesized with the temperature in the reducing atmosphere were observed as shown in Fig. 5. The MgO powder did not show any grain growth with the temperature, showing the particle size of 0.05 ± 0.01 μm at 1200 °C. The particle size in the $Mg_{0.7}Mn_{0.3}O$ and MnO powders increased with increasing temperature, showing a bigger particle size in the MnO powder. The particle morphology of the $Mg_{0.7}Mn_{0.3}O$ and MnO particles became polygonal at 1000 and 800 °C, respectively, but the MgO did not change its morphology until 1200 °C.

The grain-growth behaviors were different from those powders shown in Fig. 3, especially the MnO powder showing a sudden grain growth at 1200 °C because the atmosphere for heat treatment was different. The severe grain growth at 1200 °C in the MnO powder is due to the low activation energy for grain growth. The activation energy of MnO (about 184.7 kJ/mol) is lower than that of NiO (about 266.2 kJ/mol) [34,35]. Based on the XRD analysis and particle size observation, the most suitable heat-treatment temperature was also considered to be 800 °C for preparing the Mg–Mn-based binary powder, even though the particle size of the $Mg_{0.7}Mn_{0.3}O$ powder (0.08 ± 0.04 μm) was slightly larger than that of the MgO powder (0.06 ± 0.03 μm) at 800 °C in the reducing atmosphere, but the same as the MgO powder of 0.08 ± 0.04 μm prepared in the inert atmosphere.The crystallite size calculated from the XRD patterns using Scherrer's formula [36] is shown in Table 2 for each powder synthesized at 600, 800, and 1000 °C. When the MgO powder was heat-treated in the inert atmosphere, there was almost no difference in the crystallite size. Similarly, the crystallinity was not significantly different for the binary and NiO powders synthesized in the inert atmosphere. When the heat treatment was performed in the reducing atmosphere, the crystallite sizes for the MgO and binary powders were much smaller than those in the inert atmosphere till 800 °C, and then increased significantly at 1000 °C, except for the binary powder. The smaller crystallite size at the relatively low temperatures in the reducing atmosphere is seen as an effect of hydrogen [37].

3.2 Effects of pH and catalyst concentration

The effects of pH in the mixed solution on the powder characteristics, such as crystallinity, particle size, and particle morphology, were investigated for both binary powders with the $Mg_{0.7}M_{0.3}O$ composition after heat treatment at 1200 °C in an inert atmosphere for the Mg–Ni binary powder and in a reducing atmosphere for Mg–Mn binary powder. In the XRD

analysis, there was no difference in crystallinity with the pH value, as shown in Fig. 6, without any peak shift in both compositions, indicating that both powders were completely synthesized as the solid solution with a binary composition. However, the particle size showed a tendency to decrease with increasing pH values in the microstructure (Fig. 7), showing a polygonal morphology in all cases. In the Mg–Ni binary powder, the particle size was not much changed after showing a small change between pH 9 and pH 11, while the Mg–Mn binary powder showed a transition point between pH 11 and pH 13 in the particle size. The particle size of the Mg–Mn binary powders was larger than that of the Mg–Ni binary powders because the activation energy was low, as mentioned above [34,35]. In addition, the isoelectric points of $Mg(OH)_2$, $Ni(OH)_2$, and Mn_3O_4 would affect its nucleation behavior [38], which are pH 10–12, pH 7–8, and pH 5–6, respectively, including the atmosphere for the heat treatment. Therefore, the agglomeration phenomenon would be hindered at pH 13 above the isoelectric point, resulting in refining the particle size in both cases.

The crystallinity, particle size, and particle morphology with changing the concentration of the catalyst to 0.1, 0.5, and 1.0 M were investigated for both binary powders of $Mg_{0.7}M_{0.3}O$ composition. At that time, the pH value was fixed as 11. As shown in Fig. 8, there was no significant difference in the crystallinity with the concentration of catalyst. However, as the concentration of catalyst increased, the particle size of both $Mg_{1-x}M_xO$ powders became fine, showing the effect of the heat-treatment atmosphere (Fig. 9). The $Mg_{0.7}Mn_{0.3}O$ showed a bigger grain size than $Mg_{0.7}Ni_{0.3}O$ at all pH values. These phenomena shown in the particle size seem to be due to the faster growth rate than the nucleation rate at a relatively low concentration of catalyst [39]. In addition, it could be seen that the heat-treatment atmosphere had a great influence on the grain growth behavior of the $Mg_{0.7}M_{0.3}O$ powders synthesized by the coprecipitation method.

3.3 Simulation results with the species and content of the substitutional element

From the MD simulations, the calculated Young's modulus of MgO is 176 GPa, which is between the literature values of 130 GPa [40] and 300 GPa using a nanoindentation test [41]. In the doped MgO compounds, Young's moduli for Ni-doped MgO, or $Mg_{1-x}Ni_xO$, where x = 0.03, 0.06, and 0.12, are 171 GPa, 164 GPa, and 149 GPa, respectively. In comparison, Young's moduli for Mn-doped MgO, or $Mg_{1-x}Mn_xO$, where x = 0.03, 0.06, and 0.12, are 166 GPa, 157 GPa, and 141 GPa, respectively.

The results showed that the Young's moduli values decrease with increasing doping level. Because both Ni and Mn are transition metals, they have multiple valences, which introduce oxygen vacancies in the compound. The presence of vacancies decreases the strength of chemical bonds, essentially making the bonds "weaker." Therefore, higher doping levels reduce Young's modulus further. The difference between the doping elements Ni and Mn can be explained by the chemical strain effect [42]. As Ni^{2+} or Mn^{2+} ions substitute Mg^{2+}, the surrounding Mg^{2+} ions become distorted, causing strains in the compound. The ionic radii of Mg^{2+}, Ni^{2+}, and Mn^{2+} are 86, 83, and 97 pm, respectively [43]. Because the ionic radius difference between Mg^{2+} and Ni^{2+} is smaller than that between Mg^{2+} and Mn^{2+}, it is expected that the chemical strain in the Ni-doped MgO is less than that in the Mn-doped MgO. Therefore, the reduction in Young's modulus in the Ni-doped MgO is smaller than the case of Mn.

Regarding the simulations for XRD patterns, they were performed with the content of the substitutional element as 1.5, 3, 6, and 12% in the $Mg_{1-x}Ni_xO$ structure, which is shown in Fig. 10(A). The diffraction patterns of relative intensity against the angle of diffraction show a peak backward shift, as well as an increased intensity in the doped structures accordingly. The $Mg_{1-x}Mn_xO$ structures with the content of the substitutional element as 1.5, 3, 6, and 12% were also obtained as shown in Fig. 10(B). The peaks were shifted to a greater degree than

that for the $Mg_{1-x}Ni_xO$ structures as shown in Fig. 10(A). It is shown that the ion radius of Mn is shifted to the left because that of Mn is larger than that of Mg, and Ni is shifted to the right because the atomic radius of Ni is smaller than that of Mg, as mentioned in Section 3.1. The XRD patterns obtained with the simulation correspond quite well to those with experimental results shown in Figs. 2 and 4. Therefore, it can be confirmed that Mn and Ni, which are substitutional elements, were synthesized as a solid solution.

3.4 Reactivity with the species and content of the substitutional element

The XRD results before and after the reaction between $Mg_{1-x}M_xO$ powders and SiO_2 are shown in Figs. 11 and 12, with the species and content of the substitutional element. The MgO and amorphous SiO_2 peaks were detected before heat treatment. When only MgO was used, Mg_2SiO_4 and unreacted SiO_2 (cristobalite) were detected (Figs. 11(B-1) and 12(B-1)). In the reaction between the Mg–Ni binary powders and SiO_2, unreacted Ni was detected with Mg_2SiO_4 and unreacted SiO_2 (Fig. 11(B-3)). As the content of Ni was decreased, the peak intensity of Ni was reduced without unreacted SiO_2. However, in the case of Mg–Mn binary oxides, only Mg_2SiO_4 was synthesized by completely reacting with SiO_2 (Fig. 12(B-2) and 12(B-3)), independent of the content of Mn. This is because the electronegativity of Mn is higher than that of Ni, which is due to the strength of the ionic bonding force [44], which can be seen to correspond to the above simulation results. Therefore, MnO, which has a strong binding force, was not reduced to Mn, but NiO is considered to be precipitated as Ni because the bond with oxygen ions is broken.

The microstructure and element analysis results after the reactivity test for each composition are shown in Fig. 13. The Mg–Ni binary powders showed better reactivity than the MgO powder, enhancing the reactivity with increasing content of Ni. However, as the content of Ni was increased, the Ni element was precipitated as shown in Fig. 13(B) and

13(C), which was verified as Ni element in the element analysis and Fig. 11. On the other hand, in the Mg–Mn binary powders, as the content of Mn increased, the reaction layer around SiO_2 became thick. As can be seen from the XRD results in Fig. 12, it was confirmed that Mn was not precipitated and fully dissolved in MgO, showing a core–shell structure. Through this, it was found that the substitution by Mn element in MgO powder could make a stable binary composition and reaction layer rather than the Ni element for synthesizing Mg_2SiO_4.

Through the results above, it was possible to synthesize large quantities of powder with a uniform composition by the coprecipitation synthesis method, which is economically cheaper than the existing sol–gel process [45,46]. In addition, in the synthesis of Mg_2SiO_4, the MgO-based binary powder with a substitutional element doped into MgO would react completely to obtain a uniform Mg_2SiO_4. Furthermore, the nonuniform reactivity, which is a problem of the conventional solid-phase reaction method [47], could be improved by controlling processing parameters in the coprecipitation process.

4. Conclusions

$Mg_{1-x}M_xO$ (M = Ni and Mn) binary powders with improved reactivity were prepared by doping substitutional metal ions into MgO using the coprecipitation method. As the content of the substitutional element was increased, the diffraction patterns were shifted to higher and lower angles continuously in the $Mg_{1-x}Ni_xO$ and $Mg_{1-x}Mn_xO$ powders, respectively, showing a greater degree in the $Mg_{1-x}Mn_xO$ powder, owing to the difference of ion radius. The most suitable heat-treatment temperature was considered to be 800 °C for preparing the binary powder in both cases, based on the particle size and crystallinity, even though the particle size was dependent on the species of substitutional element and the Mn-doped binary powder showed a larger particle size than the Ni-doped one. The crystallinity and crystal size

increased as the heat-treatment temperature increased, especially in the case of $Mg_{1-x}Mn_xO$ binary composition, showing an effect of the heat-treatment atmosphere. The pH value of slurry and the concentration of catalyst did not significantly affect crystallinity, but the particle size tended to be finer as the pH value increased, indicating again that the heat-treatment atmosphere had a great influence on the grain growth behavior of the $Mg_{0.7}M_{0.3}O$ powders synthesized by the coprecipitation method. The simulation results with the species and content of the substitutional element indicated that the Mn and Ni, which are substitutional elements, were synthesized as a solid solution. The X-ray patterns obtained with the simulation corresponded quite well to those of the experimental results. As a result of analyzing the reactivity with SiO_2, unreacted SiO_2 was detected when the MgO and $Mg_{1-x}Ni_xO$ powders were applied, and Ni was precipitated in the $Mg_{1-x}Ni_xO$ binary powder. On the other hand, when the $Mg_{1-x}Mn_xO$ powder was applied for the reaction with SiO_2, only forsterite (Mg_2SiO_4) was synthesized by reacting uniformly with SiO_2. Finally, the processing parameters for synthesizing the $Mg_{1-x}M_xO$ binary powders were optimized in the coprecipitation method and the reactivity was confirmed to form Mg_2SiO_4 using the binary powders.

Acknowledgments

This work was supported by the "Human Resources Program in Energy Technology" of the Korea Institute of Energy Technology Evaluation and Planning (KETEP), granted financial resources from the Ministry of Trade, Industry and Energy, Republic of Korea (No. 20194030202450), and POSCO in 2019.

References

[1] M.H. Fathi, M. Kharaziha, Mechanically activated crystallization of phase pure nanocrystalline forsterite powders, Mater. Lett. 62 (2008) 4306–4309.

[2] C.J. Brinker, G.W. Scherer, Sol-Gel Science: The Physics and Chemistry of Sol-Gel Processing, Academic Press, Boston, 1990.

[3] D. Mishra, S. Anand, R.K. Panda, R.P. Das, Hydrothermal preparation and characterization of boehmites, Mater. Lett. 42 (2000) 38–45.

[4] J. Li, X. Sun, S. Liu, X. Li, J.G. Li, D. Huo, A homogeneous co-precipitation method to synthesize highly sinterability YAG powders for transparent ceramics, Ceram. Inter. 41 (2015) 3283–3287.

[5] B. Lee, P. Kang, K.H. Lee, J. Cho, W. Nam, W.K. Lee, N.H. Hur, Solid-state and solvent-free synthesis of azines, pyrazoles, and pyridazinones using solid hydrazine, Tetrahedron Lett. 54 (2013) 1384–1388.

[6] A.R. West, Solid State Chemistry and Its Applications, second ed., Wiley and Sons, New York, 2014.

[7] M.B.D. Mitchell, D. Jackson, P.F. James, Preparation and characterization of forsterite (Mg_2SiO_4) aerogels, J. Non-Cryst. Solids 225 (1998) 125–129.

[8] M.T. Tsai, Preparation and crystallization of forsterite fibrous gels, J. Eur. Ceram. Soc. 23(8) (2003) 1283–1291.

[9] K.X. Song and X.M. Chen, Phase evolution and microwave dielectric characteristics of Ti-substituted Mg_2SiO_4 forsterite ceramics, Mater. Lett. 62 (2008) 520–522.

[10] S. Ni, L. Chou, J. Chang, Preparation and characterization of forsterite (Mg_2SiO_4) bioceramics, Ceram. Inter. 33 (2007) 83–88.

[11] A. Saberi, B. Alinejad, Z. Negahdari, F. Kazemi, A. Almasi, A novel method to low temperature synthesis of nanocrystalline forsterite, Mat. Res. Bull. 42 (2007) 666–673.

[12] T.W. Cheng, Y.C. Ding, J.P. Chiu, A study of synthetic forsterite refractory materials using waste serpentine cutting, Miner. Eng. 15 (2002) 271–275.

[13] L. Cheng, P. Liu, X.G. Zhao, Q. Liu, H.W. Zhang, Fabrication of nanopowders by high energy ball milling and low temperature sintering of Mg_2SiO_4 microwave dielectrics, J. Alloys Compd. 513 (2012) 373–377.

[14] F. Tavangarian, R. Emadi, Mechanochemical synthesis of single phase nanocrystalline forsterite powder, Inter. J. Mod. Phys. B 24(3) (2010) 343–350.

[15] L. Chen, G. Ye, Q. Wang, B. Blanpain, A. Malfliet, M. Guo, Low temperature synthesis of forsterite from hydromagnesite and fumed silica mixture, Ceram. Inter. 41 (2015) 2234–2239.

[16] L. Chen, G. Ye, W. Zhou, J. Dijkmans, B. Sels, A. Malfliet, M. Guo, Influence of MgO precursors on mechanically activated forsterite synthesis, Ceram. Inter. 41 (2015) 12651–12657.

[17] A. Pilarska, M. Wysokowski, E. Markiewicz, T. Jesionowski, Synthesis of magnesium hydroxide and its calcinates by a precipitation method with the use of magnesium sulfate and poly(ethylene glycols), Powder Technol. 235 (2013) 148–157.

[18] J.G. Li, T. Ikegami, Y. Wang, T. Mori, Reactive ceria nanopowders via carbonate precipitation, J. Am. Ceram. Soc. 85(9) (2002) 2376–2378.

[19] E. Matijevic, W.P. Hsu, Preparation and properties of monodispersed colloidal particles of lanthanide compounds: I. gadolinium, europium, terbium, samarium and cerium(III), J. Colloid Interface Sci. 118(2) (1987) 506–523.

[20] A.H. Lu, E.L. Salabas, F. Schüth, Magnetic nanoparticles: synthesis, protection, functionalization, and application, Angew. Chem. Int. Ed. 46 (2007) 1222–1244.

[21] M. Rezaei, M. Khajenoori, B. Nematollhi, Preparation of nanocrystalline MgO by surfactant assisted precipitation method, Mat. Res. Bull. 46 (2011) 1632–1637.

[22] S. Da Ros, M.D. Jones, D. Mattia, J.C. Pinto, M. Schwaab, F.B. Noronha, S.A. Kondrat, T.C. Clarke, S.H. Taylor, Ethanol to 1,3-butadiene conversion by using ZrZn-containing MgO/SiO2 systems prepared by co-precipitation and effect of catalyst acidity modification, ChemCatChem 8 (2016) 2376–2386.

[23] F.P. Glasser, E.F. Osborn, The ternary system MgO-MnO-SiO_2, J. Am. Ceram. Soc. 43(3)

(1960) 132–140.

[24] W.C. Hahn, A. Muan, Activities of the oxide components in NiO-MnO-MgO solid solutions, Mat. Res. Bull. 5 (1970) 955–964.

[25] T.S. Liu, R.J. Stokes, C.H. Li, Fabrication and plastic behavior of single-crystal MgO-NiO and MO-MnO solid-solution alloys, J. Am. Ceram. Soc. 47(6) (1964) 276–279.

[26] A.L. Patterson, The Scherrer formula for X-ray particle size determination, Phys. Rev. 56(10) (1939) 978–982.

[27] M. Khatamiana, M. Irani, Preparation and characterization of nanosized ZSM-5 zeolite using kaolin and investigation of kaolin content, crystallization time and temperature changes on the size and crystallinity of products, J. Iran. Chem. Soc. 6(1) (2009) 187–194.

[28] A. Pedone, G. Malavasi, M.C. Menziani, A.N. Cormack, U. Segre, A new self-consistent empirical interatomic potential model for oxides, silicates, and silica-based glasses, J. Phys. Chem. B. 110(24) (2006) 11780–11795.

[29] S. Plimpton, Fast parallel algorithms for short-range molecular dynamics, J. Comput. Phys. 117 (1995) 1–19.

[30] M.Z. Said, Effect of gadolinium substitutions on the structure and electrical conductivity of Ni-ferrite, Mater. Lett. 34 (1998) 305–307.

[31] V.S. Escribano, E.F. Lopez, M. Panizza, C. Resini, J.M.G. Amores, G. Busca, Characterization of cubic ceria-zirconia powders by X-ray diffraction and vibrational and electronic spectroscopy, Solid State Sci. 5 (2003) 1369–1376.

[32] W. Hume-Rothery, Atomic Theory for Students of Metallurgy, The Institute of Metals, London, 1969 (fifth reprint).

[33] J.H. Moon, M. Awano, H. Takagi, Y. Fujishiro, Synthesis of nanocrystalline manganese oxide powders: influence of hydrogen peroxide on particle characteristics, J. Mater. Res. 14(12) (1999) 4594–4601.

[34] B. Malecka, E.D. Ciesla, P.K. Olszewski, Kinetics of thermal decomposition of manganese(II) oxalate, J. Therm. Anal. Calorim. 74 (2003) 485–490.

[35] R. Alizadeh, E. Jamshidi, H.A. Ebrahim, Kinetic study of nickel oxide reduction by methane, J. Eng. Technol. 30(8) (2007) 1123–1128.

[36] J. Chen, M. Yao, X. Wang, Investigation of transition metal ion doping behaviors on TiO_2 nanoparticles, J. Nanopart. Res. 10 (2008) 163–171.

[37] B. Wong, J.A. Pask, Experimental analysis of sintering of MgO compacts, J. Am. Ceram. Soc. 62(3-4) (1979) 141–146.

[38] A. Pilarska, M. Nowacka, K. Pilarski, D. Paukszta, L. Klapiszewski, T. Jesionowski, Preparation and characterisation of unmodified and poly(ethylene glycol) grafted magnesium hydroxide, Physicochem. Probl. Miner. Process. 49(2) (2013) 701–712.

[39] Y.U. Ahn, E.J. Kim, H.T. King, S.H. Hahn, Variation of structural and optical properties of sol-gel TiO_2 thin films with catalyst concentration and calcination temperature, Mater. Lett. 57 (2003) 4660–4666.

[40] R. Gaillac, P. Pullumbi, F.X. Coudert, ELATE: an open-source online application for analysis and visualization of elastic tensors, J. Phys. Condens. Matter. 28 (2016) 275201–275205.

[41] D. Caceres, I. Vergara, R. Gonzalez, Y. Chen, Hardness and elastic modulus from nanoindentations in nominally pure and doped MgO single crystals, Philos. Mag. Lett. 82(6) (2002) 1159–1171.

[42] E. Watchtel, I. Lubomirsky, The elastic modulus of pure and doped ceria, Scr. Mater. 65 (2011) 112–117.

[43] Ionic radius (https://en.wikipedia.org/wiki/Ionic_radius#:~:text=Ionic%20radii%20are%20typically %20given,into%20consideration%20the%20solvation%20shell., accessed July 2020).

[44] A.L. Allred, Electronegativity values from thermochemical data, J. Inorg. Nucl. Chem. 17 (1961) 215–221.

[45] S. Sembiring, A. Ritanto, W. Simanjuntak, R. Situmeang, Effect of MgO-SiO_2 ratio on the forsterite (Mg_2SiO_4) precursors characteristics derived from amorphous rice husk silica, Orient. J. Chem. 33(4) (2017) 1828–1836.

[46] S.G. Son, J.H. Lee, S.H. Lee, Y.D. Kim, Low temperature synthesis of forsterite powders by the geopolymer technique, J. Korean Ceram. Soc. 46(3) (2009) 242–248.

[47] J.A. Tangeman, B.L. Phillips, A. Navrotsky, J.K.R. Weber, Vitreous forsterite (Mg_2SiO_4): synthesis, structure, and thermochemistry, Geophys. Res. Lett. 28(13) (2001) 2517–2520.

Table captions

Table 1. Mole ratio of precursors for preparing $Mg_{1-x}Ni_xO$ and $Mg_{1-x}Mn_xO$ powders

Table 2. Average crystallite size of $Mg_{1-x}M_xO$ powders according to the content of M (M = Ni, Mn) and heat-treatment temperature

Figure captions

Fig. 1. Schematic diagram for preparing the binary powders of $Mg_{1-x}Ni_xO$ and $Mg_{1-x}Mn_xO$ using the precursors of metal chlorides.

Fig. 2. XRD results for the synthesized MgO, $Mg_{1-x}Ni_xO$, and NiO powders with heat-treatment temperature: (A) before heat treatment, (B) 600 °C, (D) 800 °C, (C) 1000 °C, and (E) 1200 °C. Each number indicates the composition of powders shown in Table 1.

Fig. 3. Particle size and morphology of synthesized powders after heat treatment: (A) 600 °C, (B) 800 °C, (C) 1000 °C, and (D) 1200 °C. Each number indicates the MgO, $Mg_{0.7}Ni_{0.3}O$, and NiO powders.

Fig. 4. XRD results for the synthesized MgO, $Mg_{1-x}Mn_xO$, and MnO powders with heat-treatment temperature: (A) before heat treatment, (B) 600 °C, (D) 800 °C, (C) 1000 °C, and (E) 1200 °C. Each number indicates the composition of powders shown in Table 1.

Fig. 5. Particle size and morphology of synthesized powders after heat treatment: (A) 600 °C, (B) 800 °C, (C) 1000 °C, and (D) 1200 °C. Each number indicates the MgO, $Mg_{0.7}Mn_{0.3}O$, and MnO powders.

Fig. 6. Variation of XRD results for $Mg_{0.7}M_{0.3}O$ powder with the pH value: (A) $Mg_{0.7}Ni_{0.3}O$ and (B) $Mg_{0.7}Mn_{0.3}O$. Each number indicates the pH values of 9, 11, and 13.

Fig. 7. Particle size and morphology for $Mg_{0.7}M_{0.3}O$ powder synthesized with the pH value: (A) $Mg_{0.7}Ni_{0.3}O$ and (B) $Mg_{0.7}Mn_{0.3}O$. Each number indicates the pH values of 9, 11, and 13.

Fig. 8. XRD results for $Mg_{0.7}M_{0.3}O$ powder synthesized with the concentration of catalyst: (A) $Mg_{0.7}Ni_{0.3}O$ and (B) $Mg_{0.7}Mn_{0.3}O$. Each number indicates 0.1, 0.5, and 1.0 M.

Fig. 9. Particle size and morphology for $Mg_{0.7}M_{0.3}O$ powder synthesized with the concentration of catalyst: (A) $Mg_{0.7}Ni_{0.3}O$ and (B) $Mg_{0.7}Mn_{0.3}O$. Each number indicates 0.1, 0.5, and 1.0 M.

Fig. 10. XRD results obtained from simulation for MgO-based binary powders: (A) $Mg_{1-x}Ni_xO$ and (B) $Mg_{1-x}Mn_xO$. The red, black, green, blue, and yellow patterns in each figure indicate MgO, $Mg_{0.985}M_{0.015}O$, $Mg_{0.97}M_{0.03}O$, $Mg_{0.94}M_{0.06}O$, and $Mg_{0.88}M_{0.12}O$, respectively.

Fig. 11. XRD results before and after the reaction between $Mg_{1-x}Ni_xO$ and SiO_2: (A) before reaction and (B) after reaction. Each number indicates MgO + SiO_2, $Mg_{0.9}Ni_{0.1}O$ + SiO_2, and $Mg_{0.7}Ni_{0.3}O$ + SiO_2.

Fig. 12. XRD results before and after the reaction between $Mg_{1-x}Mn_xO$ and SiO_2: (A) before reaction and (B) after reaction. Each number indicates MgO + SiO_2, $Mg_{0.9}Mn_{0.1}O$ + SiO_2, and $Mg_{0.7}Mn_{0.3}O$ + SiO_2.

Fig. 13. Microstructure and element analysis after the reaction between $Mg_{1-x}M_xO$ powders and SiO_2: (A) MgO + SiO_2, (B) $Mg_{0.9}Ni_{0.1}O$ + SiO_2, (C) $Mg_{0.7}Ni_{0.3}O$ + SiO_2, (D) $Mg_{0.9}Mn_{0.1}O$ + SiO_2, and (E) $Mg_{0.7}Mn_{0.3}O$ + SiO_2.

Figures

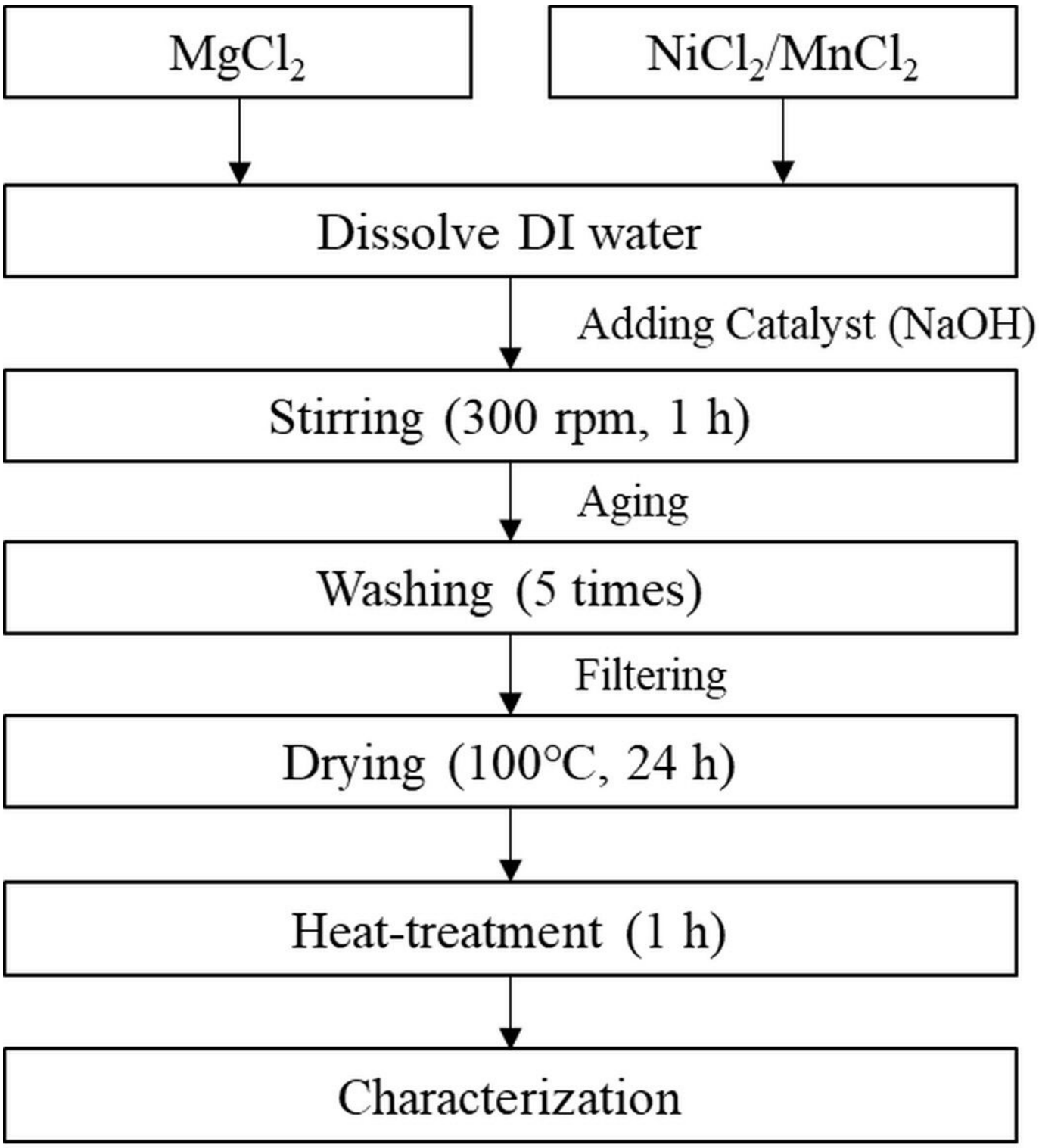

Figure 1

Schematic diagram for preparing the binary powders of Mg1−xNixO and Mg1−xMnxO using the precursors of metal chlorides.

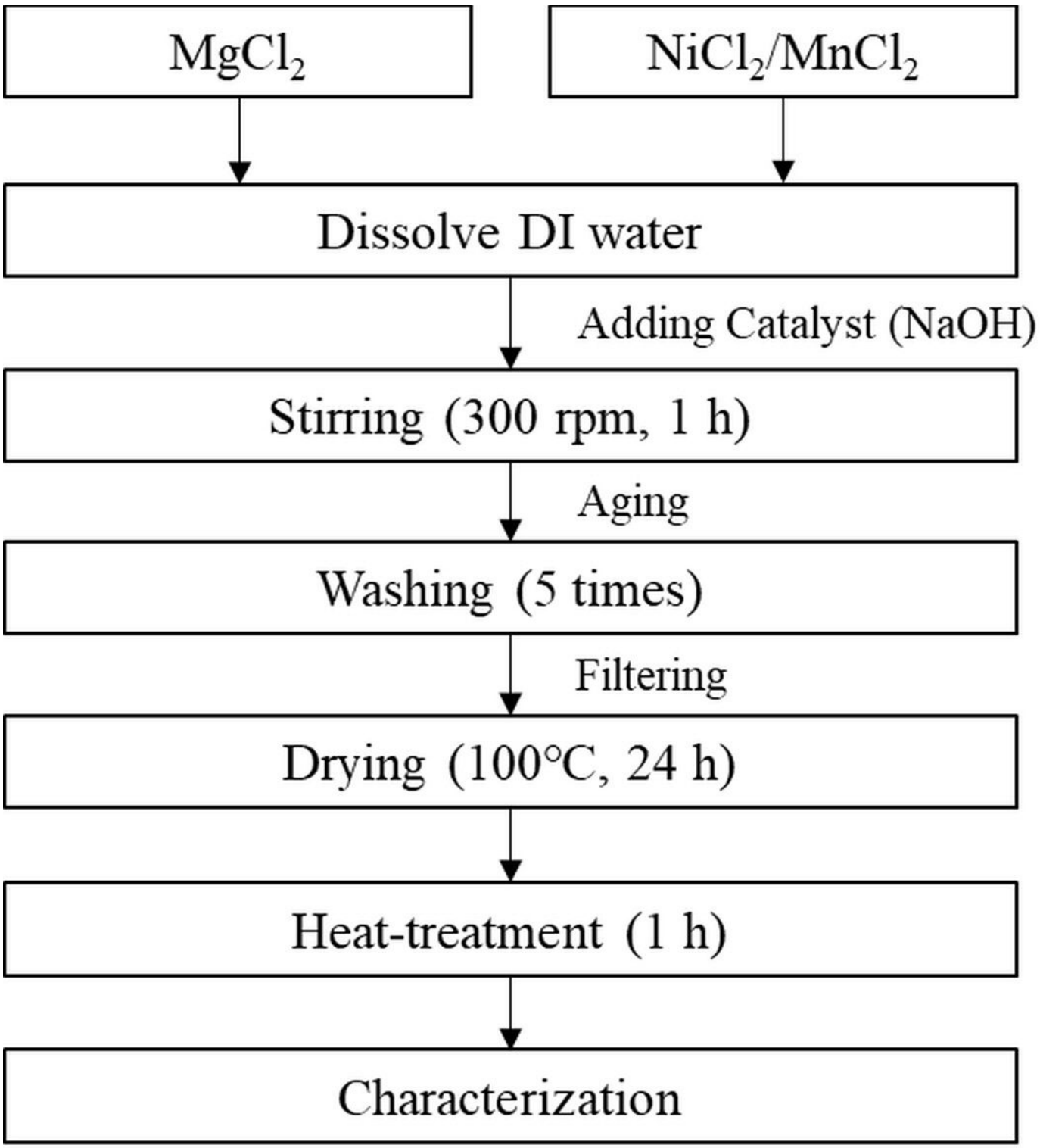

Figure 1

Schematic diagram for preparing the binary powders of Mg1−xNixO and Mg1−xMnxO using the precursors of metal chlorides.

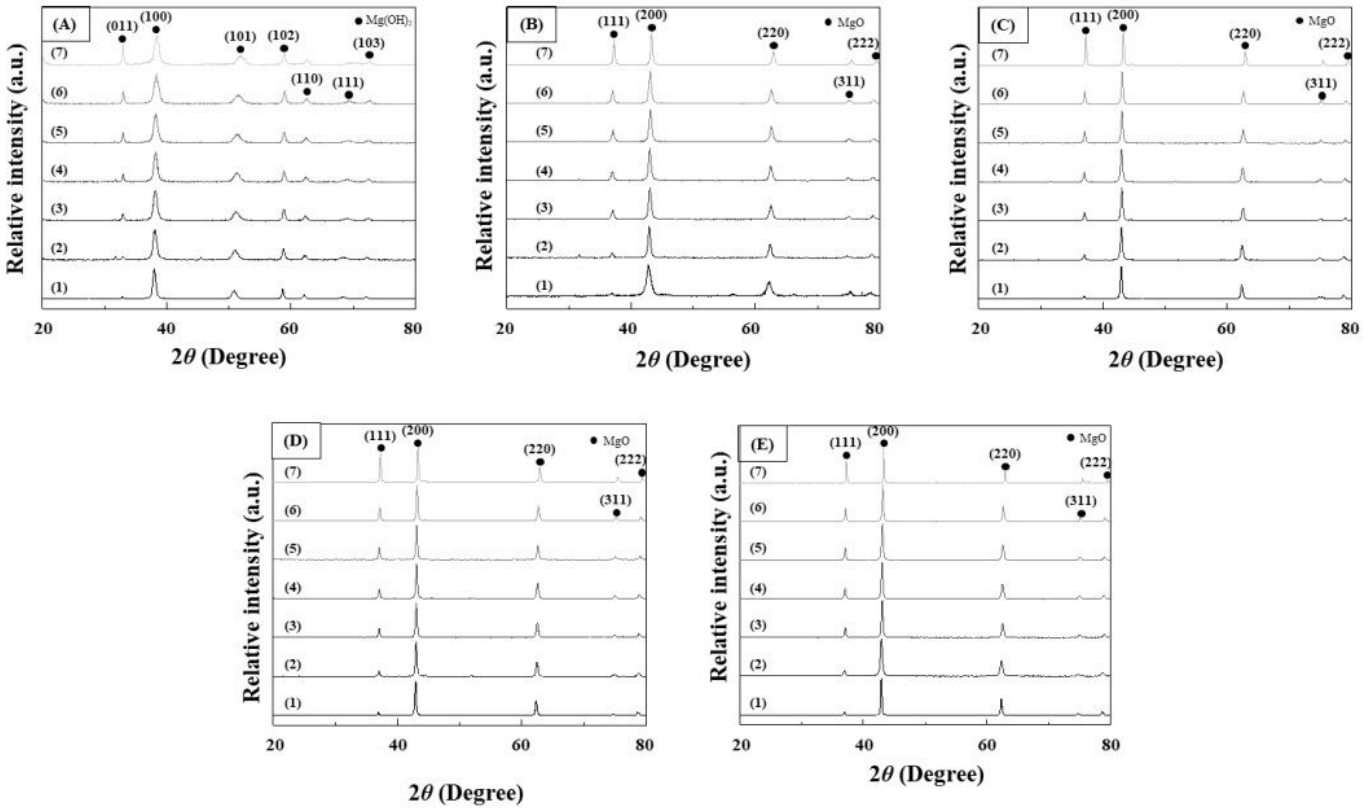

Figure 2

XRD results for the synthesized MgO, Mg1−xNixO, and NiO powders with heat-treatment temperature: (A) before heat treatment, (B) 600 °C, (D) 800 °C, (C) 1000 °C, and (E) 1200 °C. Each number indicates the composition of powders shown in Table 1.

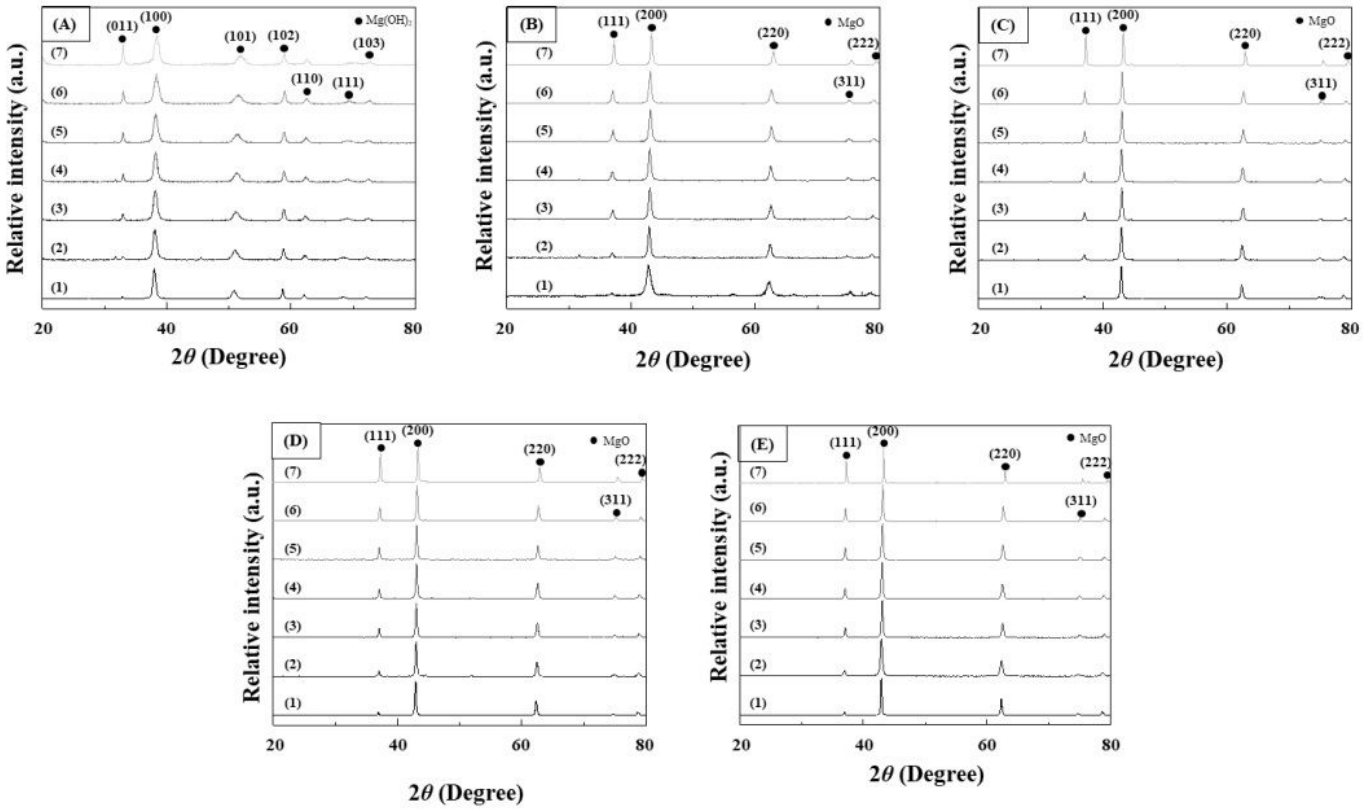

Figure 2

XRD results for the synthesized MgO, Mg1−xNixO, and NiO powders with heat-treatment temperature: (A) before heat treatment, (B) 600 °C, (D) 800 °C, (C) 1000 °C, and (E) 1200 °C. Each number indicates the composition of powders shown in Table 1.

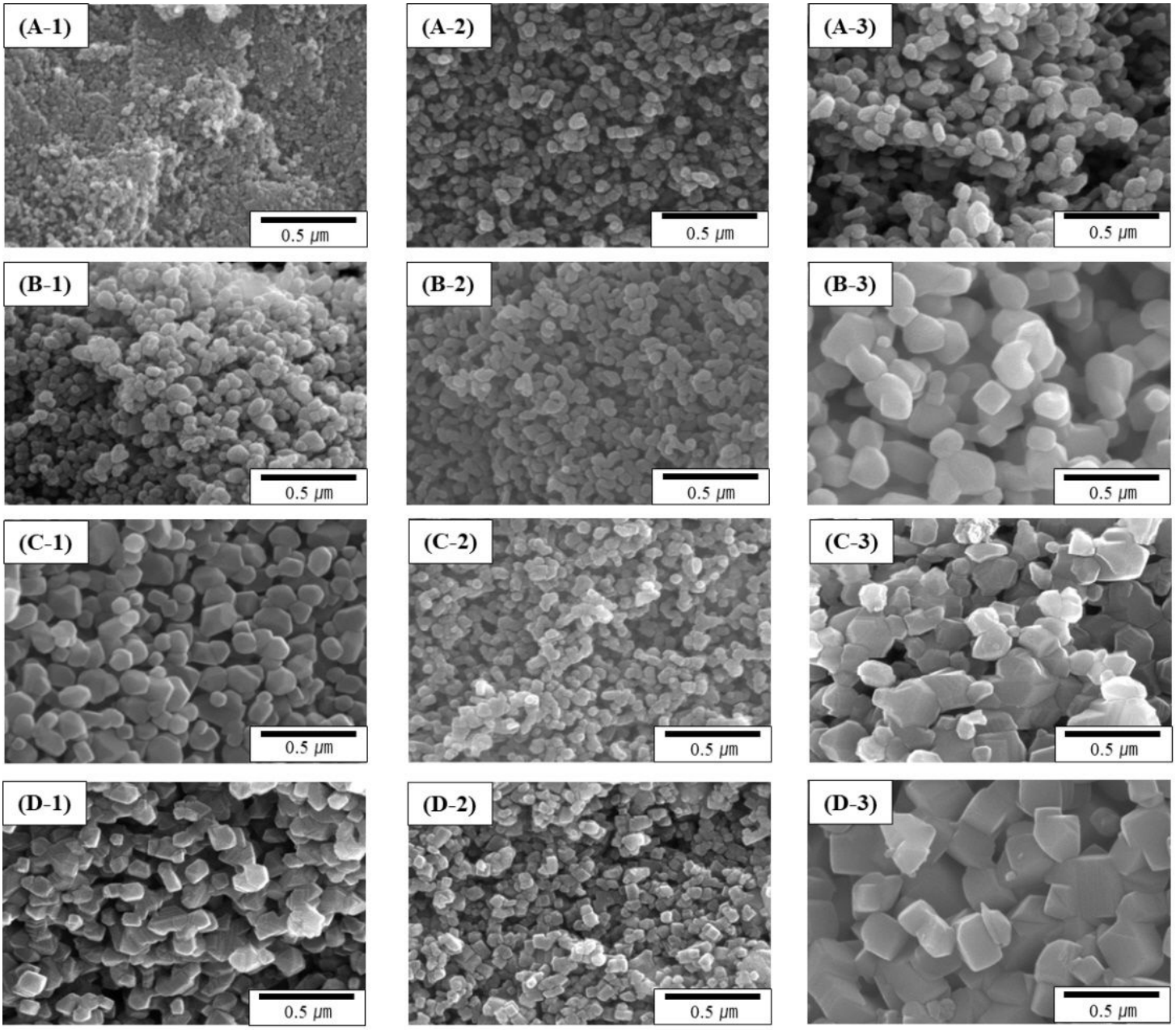

Figure 3

Particle size and morphology of synthesized powders after heat treatment: (A) 600 °C, (B) 800 °C, (C) 1000 °C, and (D) 1200 °C. Each number indicates the MgO, Mg0.7Ni0.3O, and NiO powders.

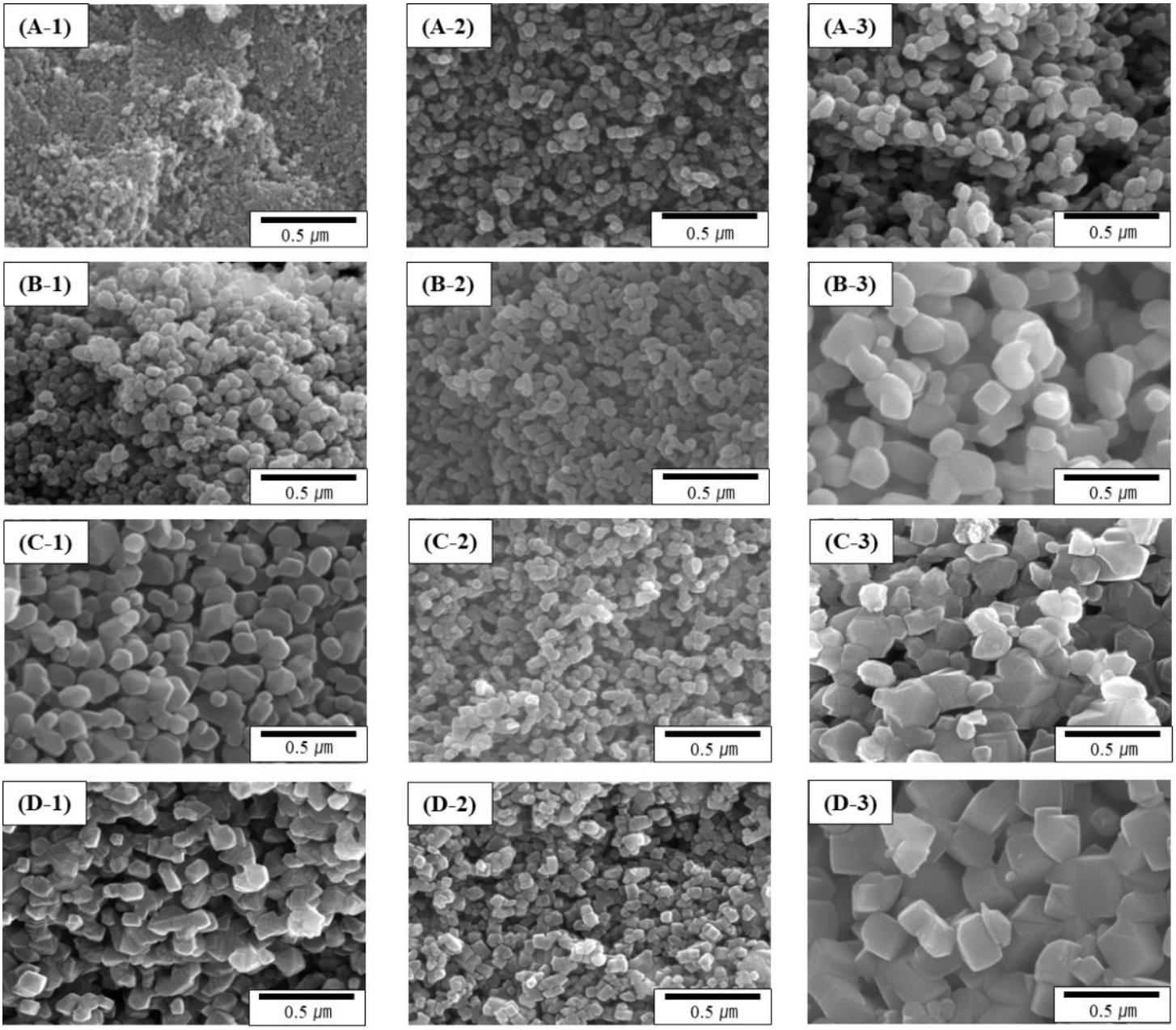

Figure 3

Particle size and morphology of synthesized powders after heat treatment: (A) 600 °C, (B) 800 °C, (C) 1000 °C, and (D) 1200 °C. Each number indicates the MgO, Mg0.7Ni0.3O, and NiO powders.

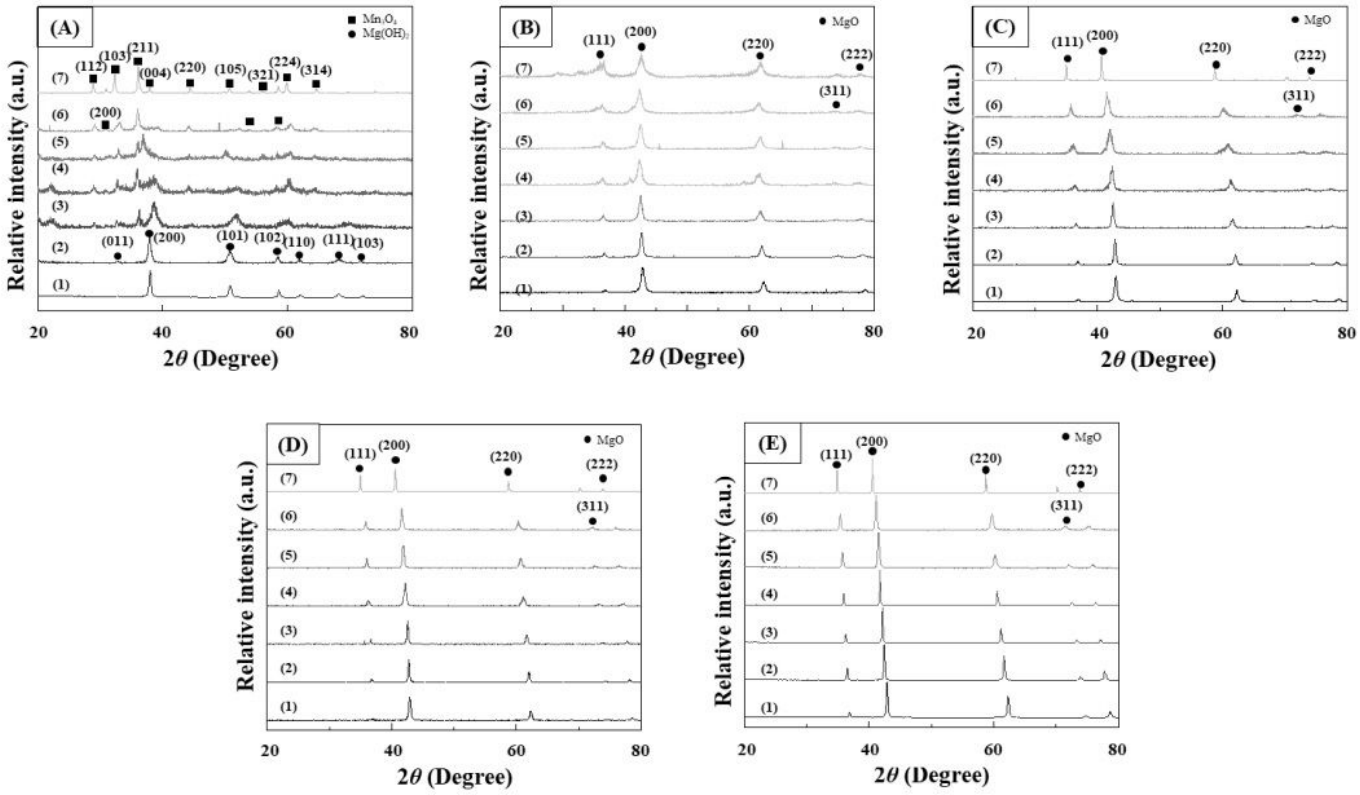

Figure 4

XRD results for the synthesized MgO, Mg1−xMnxO, and MnO powders with heat-treatment temperature: (A) before heat treatment, (B) 600 °C, (D) 800 °C, (C) 1000 °C, and (E) 1200 °C. Each number indicates the composition of powders shown in Table 1.

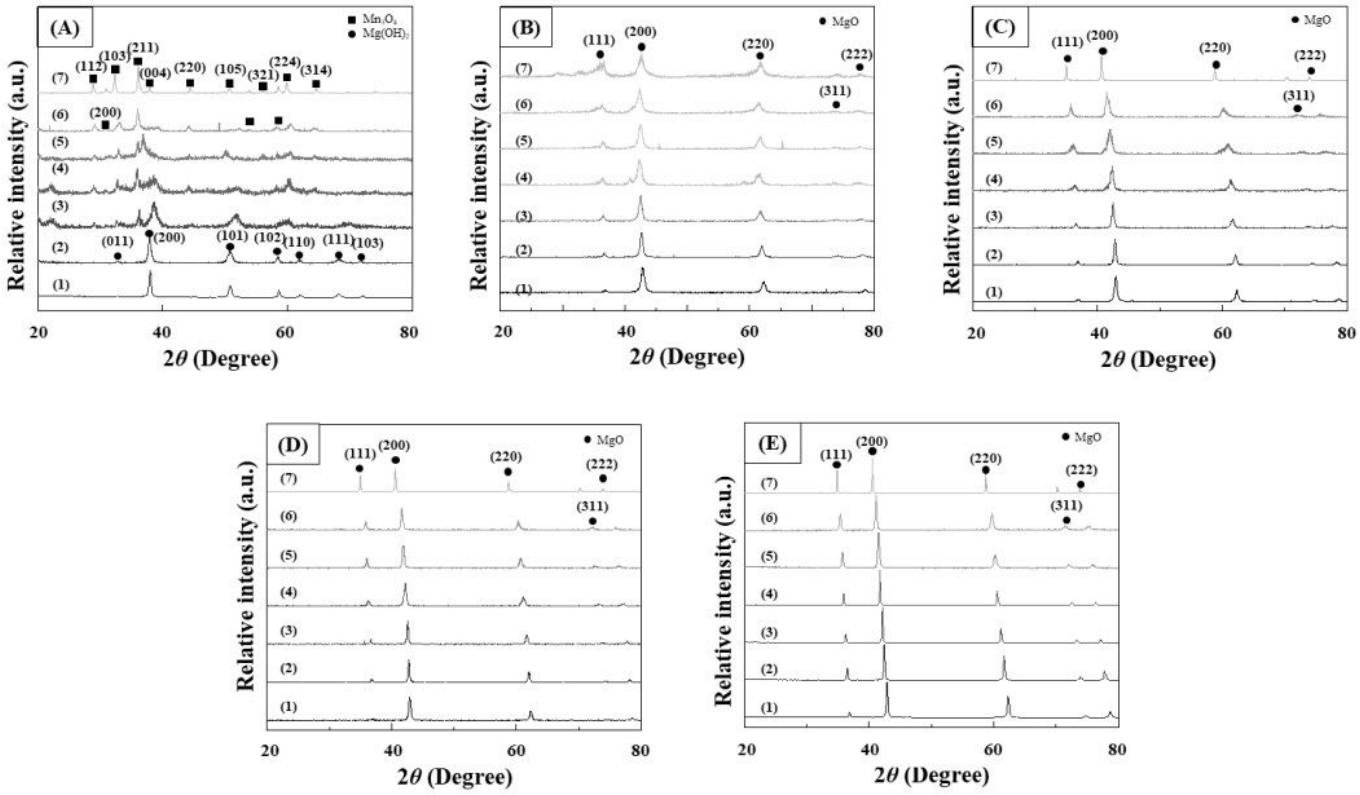

Figure 4

XRD results for the synthesized MgO, Mg1−xMnxO, and MnO powders with heat-treatment temperature: (A) before heat treatment, (B) 600 °C, (D) 800 °C, (C) 1000 °C, and (E) 1200 °C. Each number indicates the composition of powders shown in Table 1.

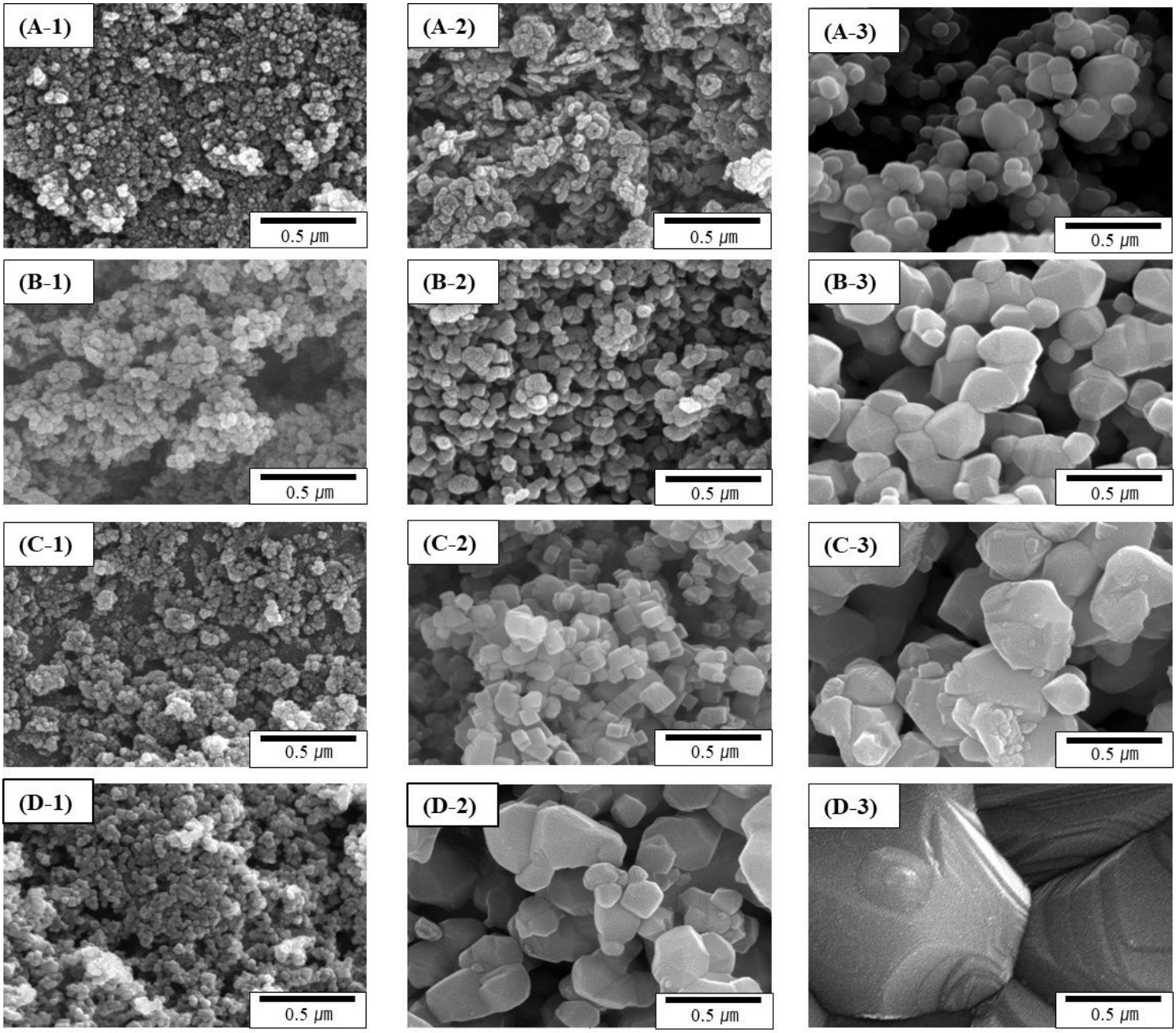

Figure 5

Particle size and morphology of synthesized powders after heat treatment: (A) 600 °C, (B) 800 °C, (C) 1000 °C, and (D) 1200 °C. Each number indicates the MgO, Mg0.7Mn0.3O, and MnO powders.

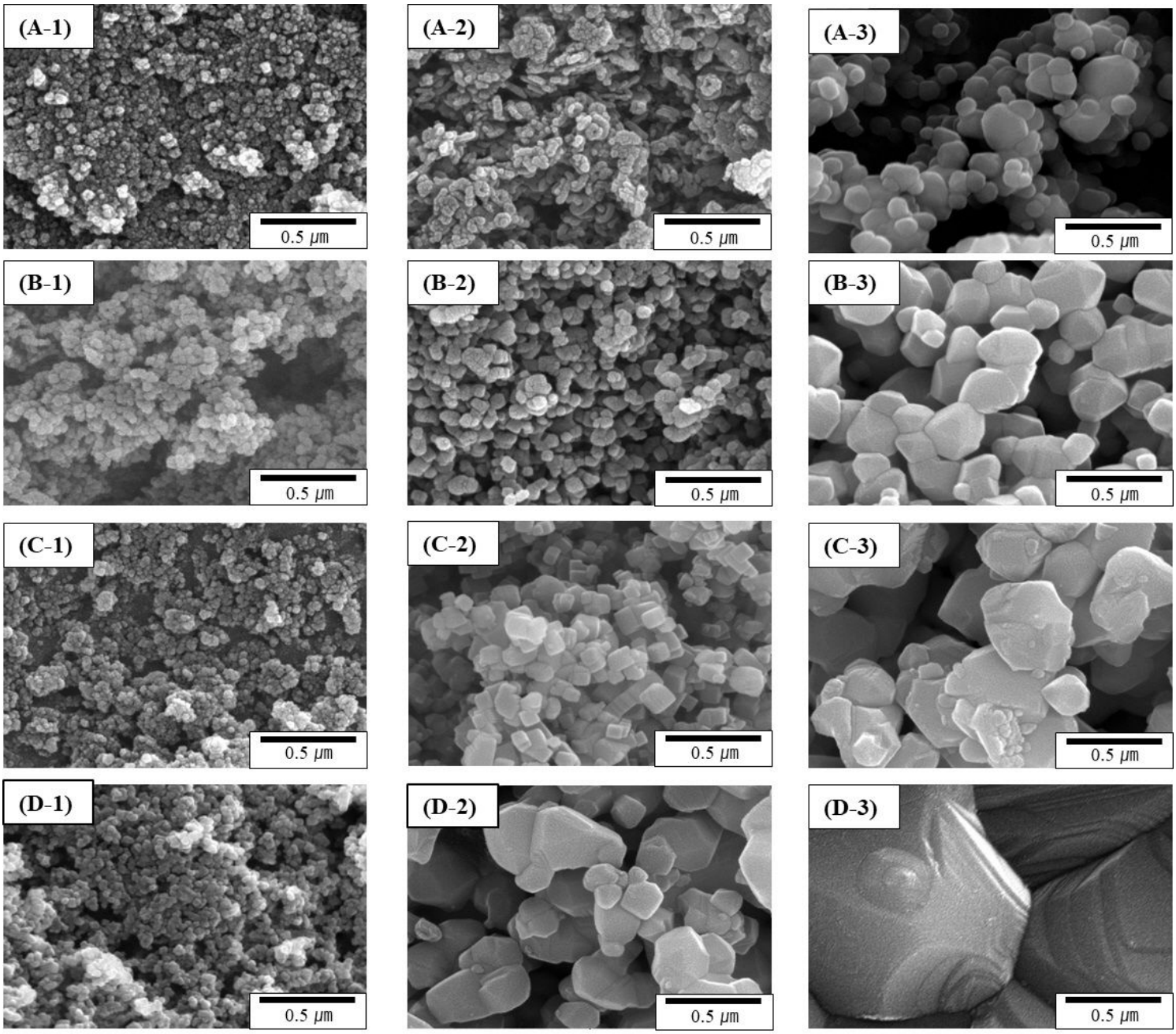

Figure 5

Particle size and morphology of synthesized powders after heat treatment: (A) 600 °C, (B) 800 °C, (C) 1000 °C, and (D) 1200 °C. Each number indicates the MgO, Mg0.7Mn0.3O, and MnO powders.

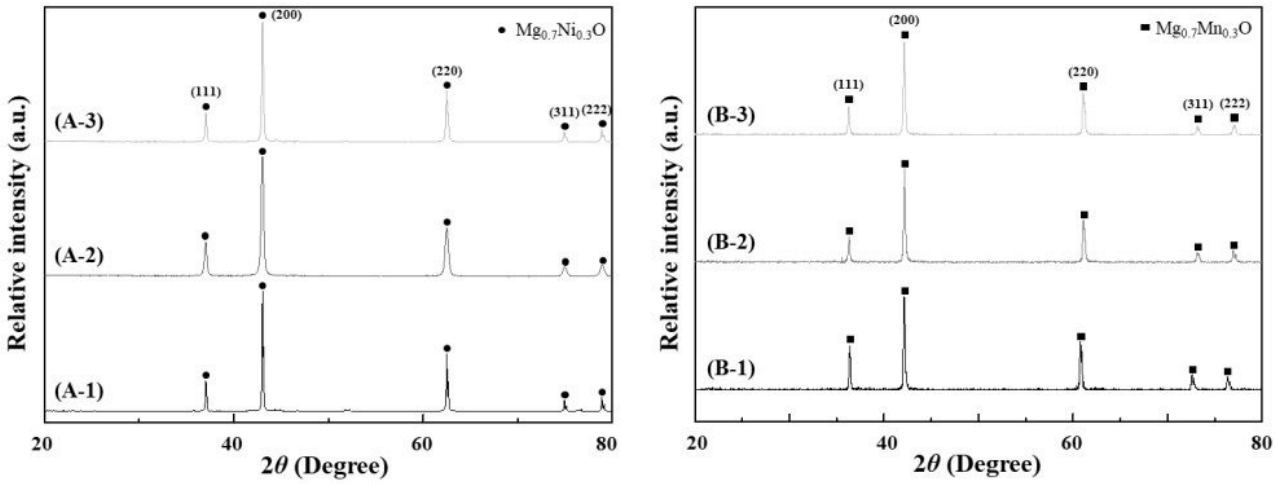

Figure 6

Variation of XRD results for Mg0.7M0.3O powder with the pH value: (A) Mg0.7Ni0.3O and (B) Mg0.7Mn0.3O. Each number indicates the pH values of 9, 11, and 13.

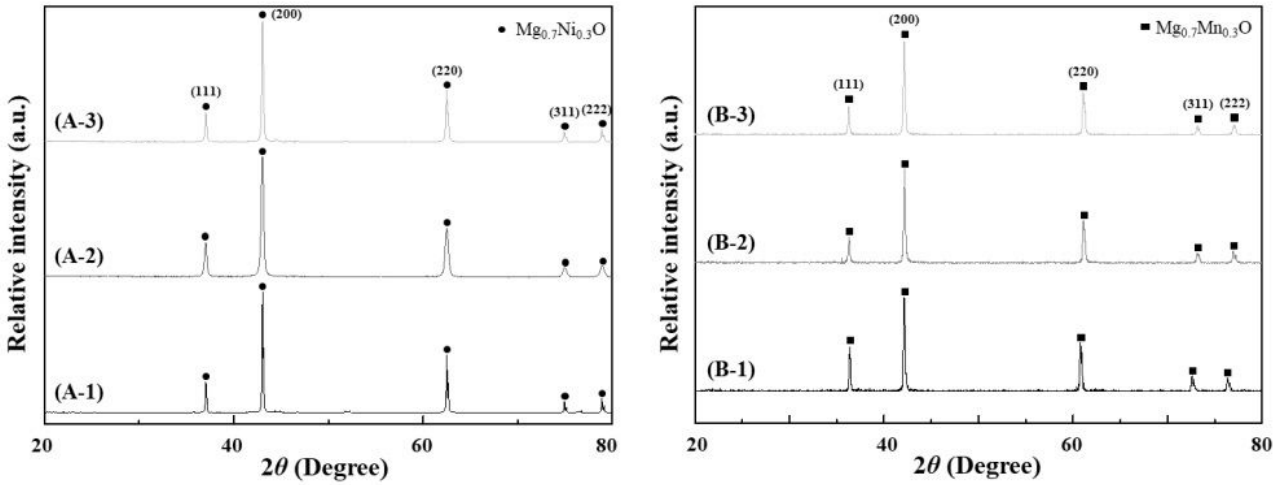

Figure 6

Variation of XRD results for Mg0.7M0.3O powder with the pH value: (A) Mg0.7Ni0.3O and (B) Mg0.7Mn0.3O. Each number indicates the pH values of 9, 11, and 13.

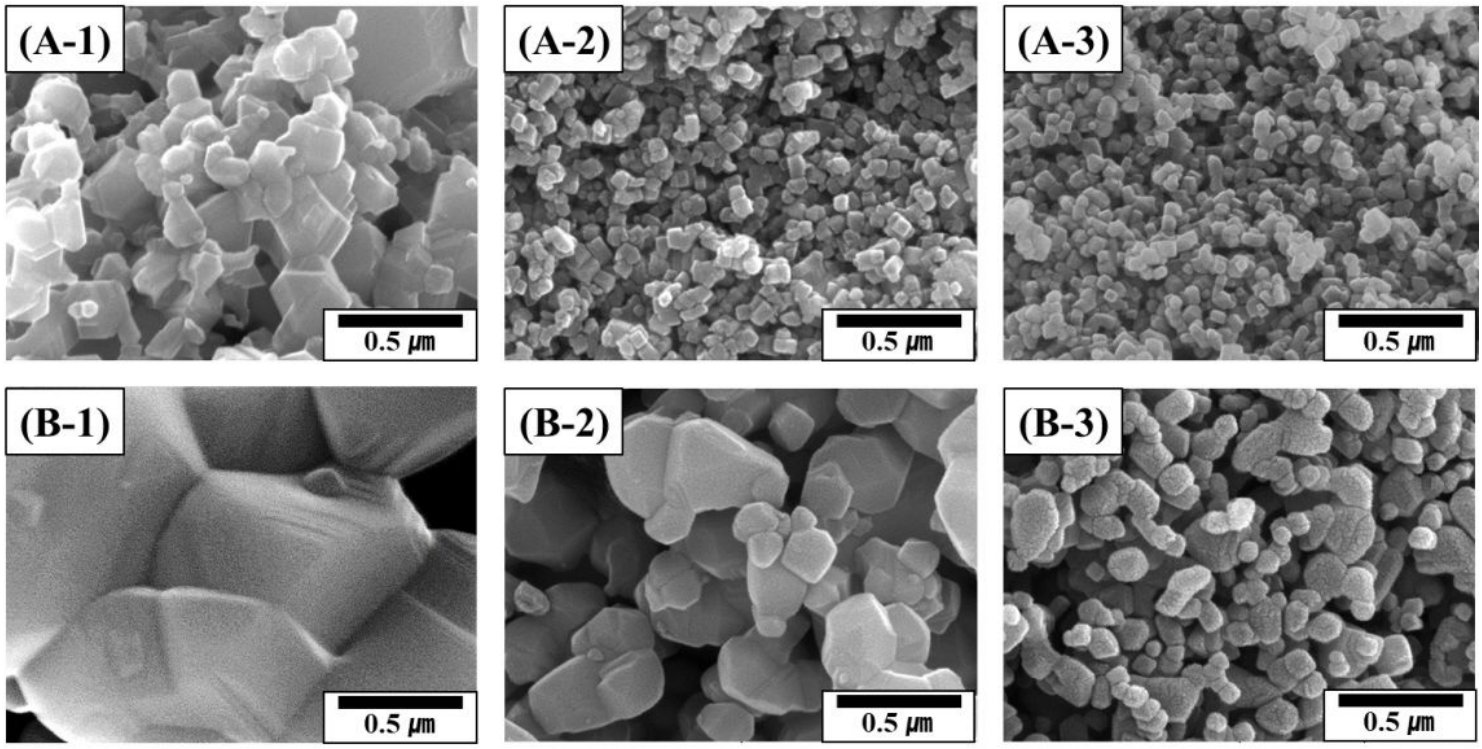

Figure 7

Particle size and morphology for Mg0.7M0.3O powder synthesized with the pH value: (A) Mg0.7Ni0.3O and (B) Mg0.7Mn0.3O. Each number indicates the pH values of 9, 11, and 13.

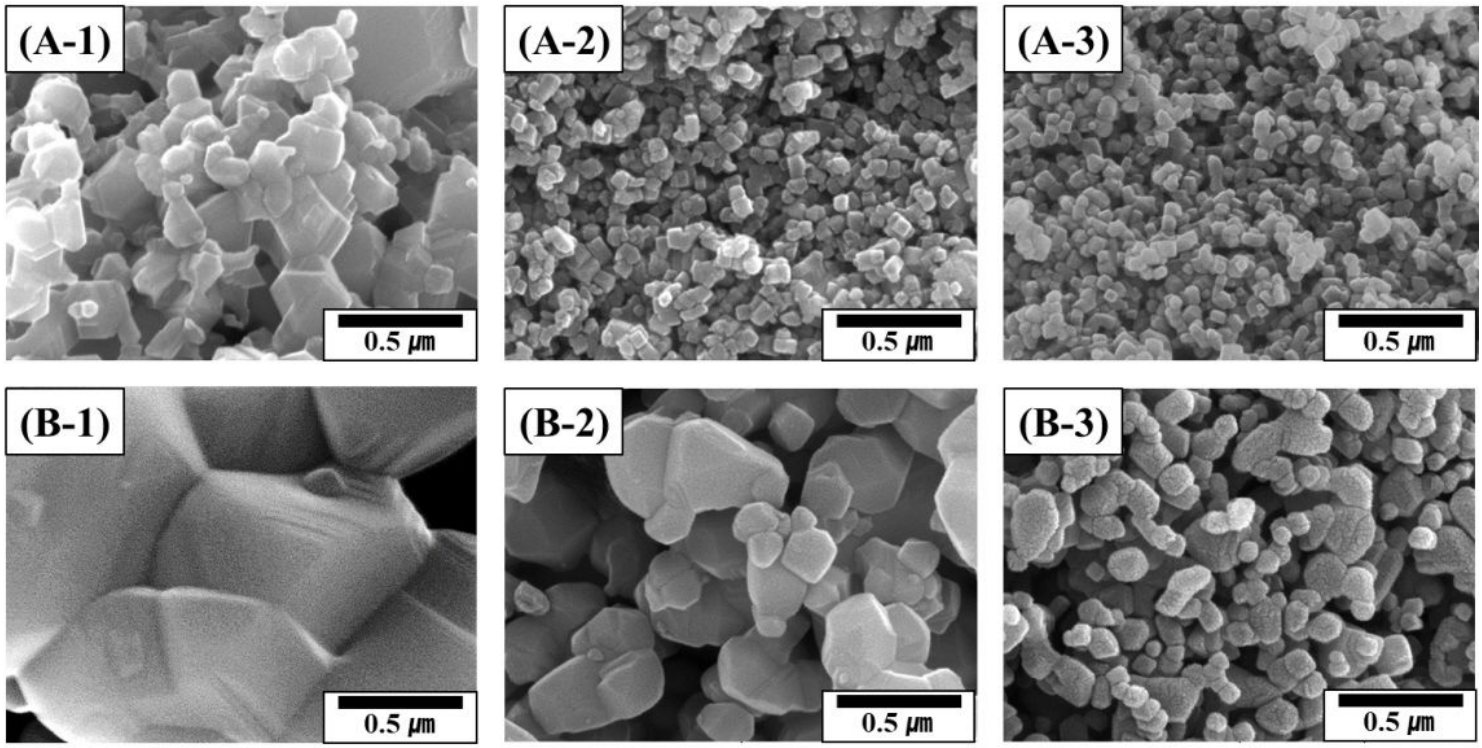

Figure 7

Particle size and morphology for Mg0.7M0.3O powder synthesized with the pH value: (A) Mg0.7Ni0.3O and (B) Mg0.7Mn0.3O. Each number indicates the pH values of 9, 11, and 13.

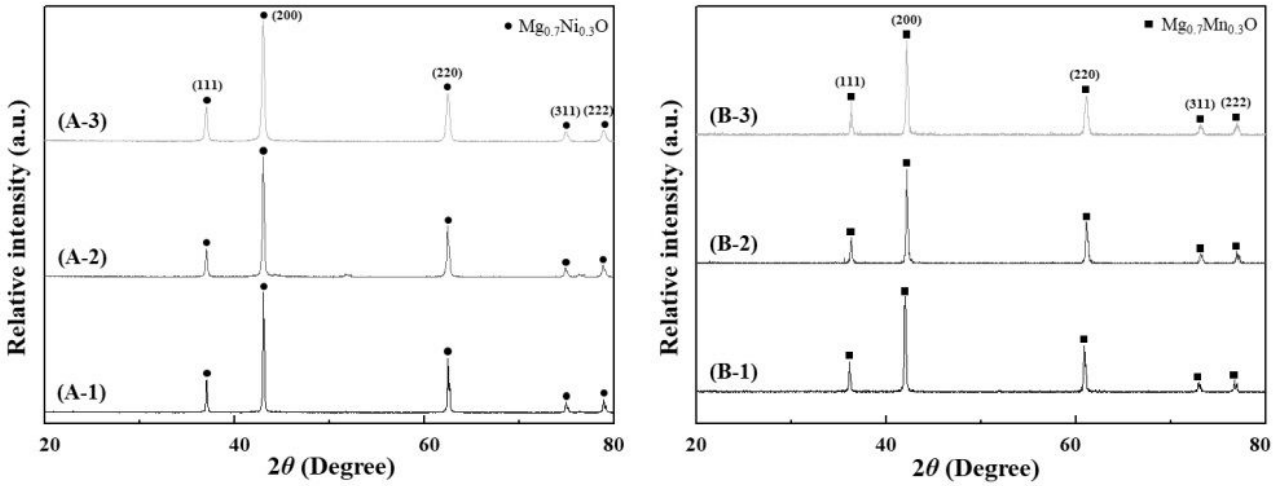

Figure 8

XRD results for Mg0.7M0.3O powder synthesized with the concentration of catalyst: (A) Mg0.7Ni0.3O and (B) Mg0.7Mn0.3O. Each number indicates 0.1, 0.5, and 1.0 M.

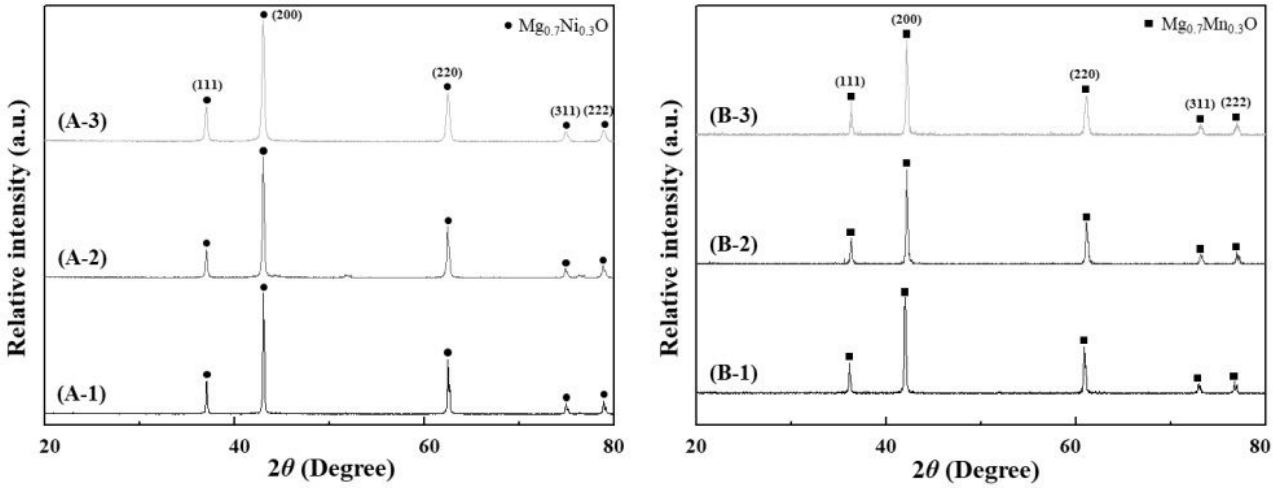

Figure 8

XRD results for Mg0.7M0.3O powder synthesized with the concentration of catalyst: (A) Mg0.7Ni0.3O and (B) Mg0.7Mn0.3O. Each number indicates 0.1, 0.5, and 1.0 M.

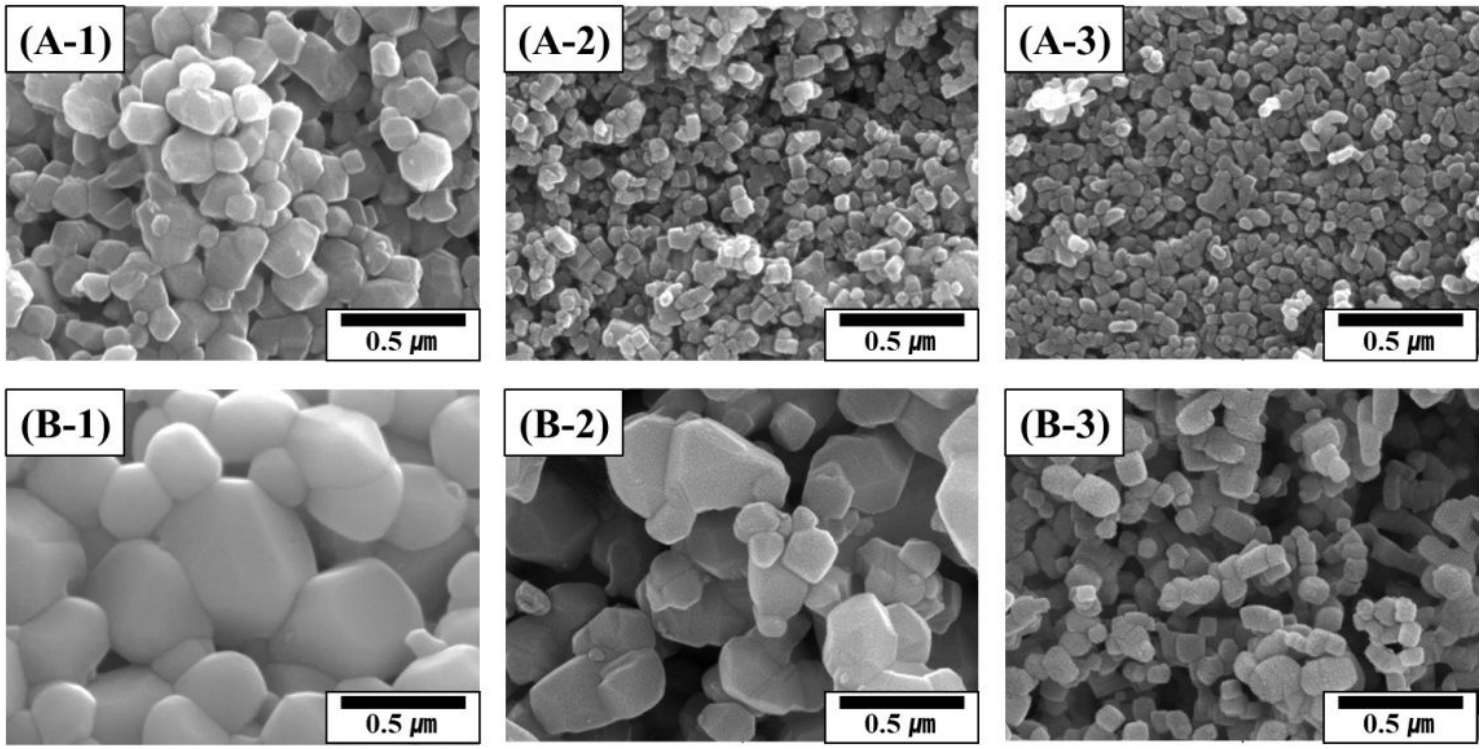

Figure 9

Particle size and morphology for Mg0.7M0.3O powder synthesized with the concentration of catalyst: (A) Mg0.7Ni0.3O and (B) Mg0.7Mn0.3O. Each number indicates 0.1, 0.5, and 1.0 M.

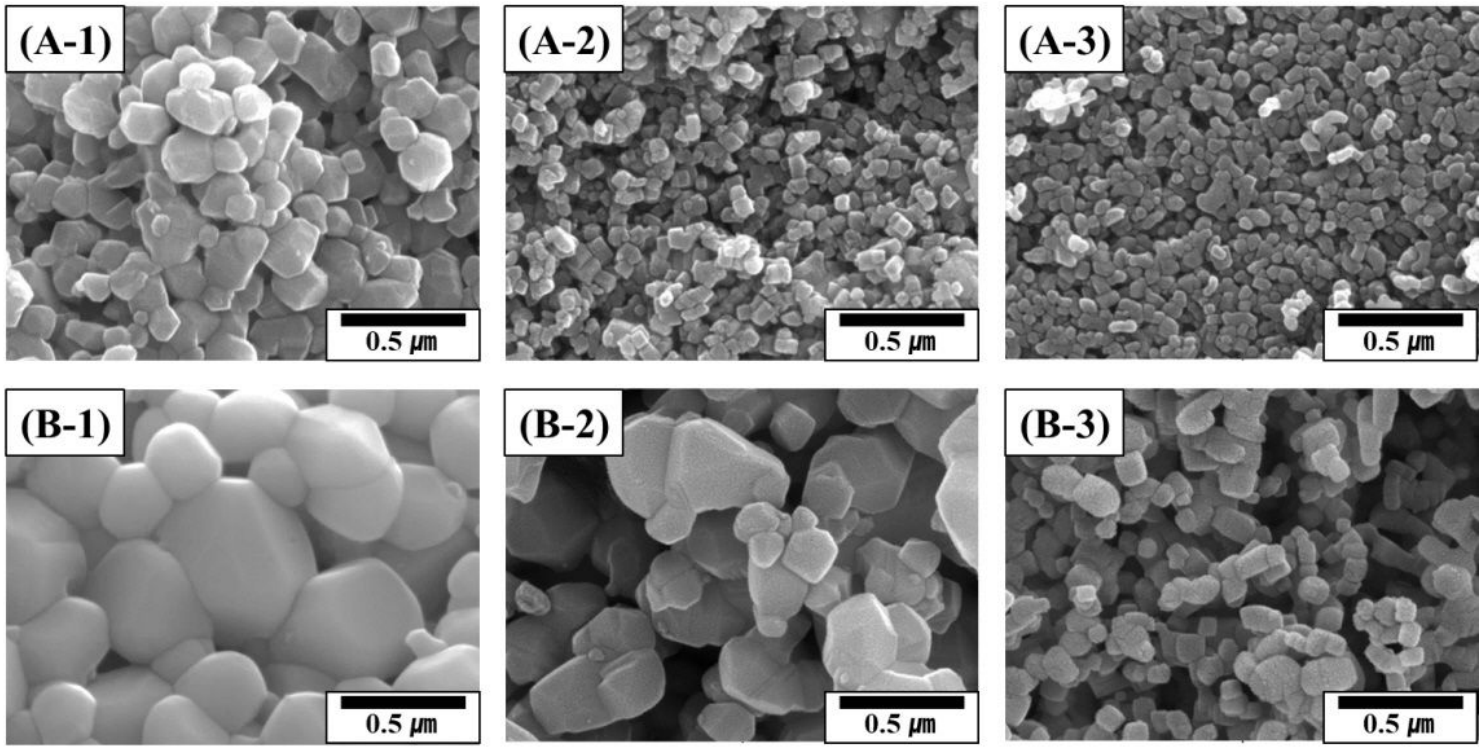

Figure 9

Particle size and morphology for Mg0.7M0.3O powder synthesized with the concentration of catalyst: (A) Mg0.7Ni0.3O and (B) Mg0.7Mn0.3O. Each number indicates 0.1, 0.5, and 1.0 M.

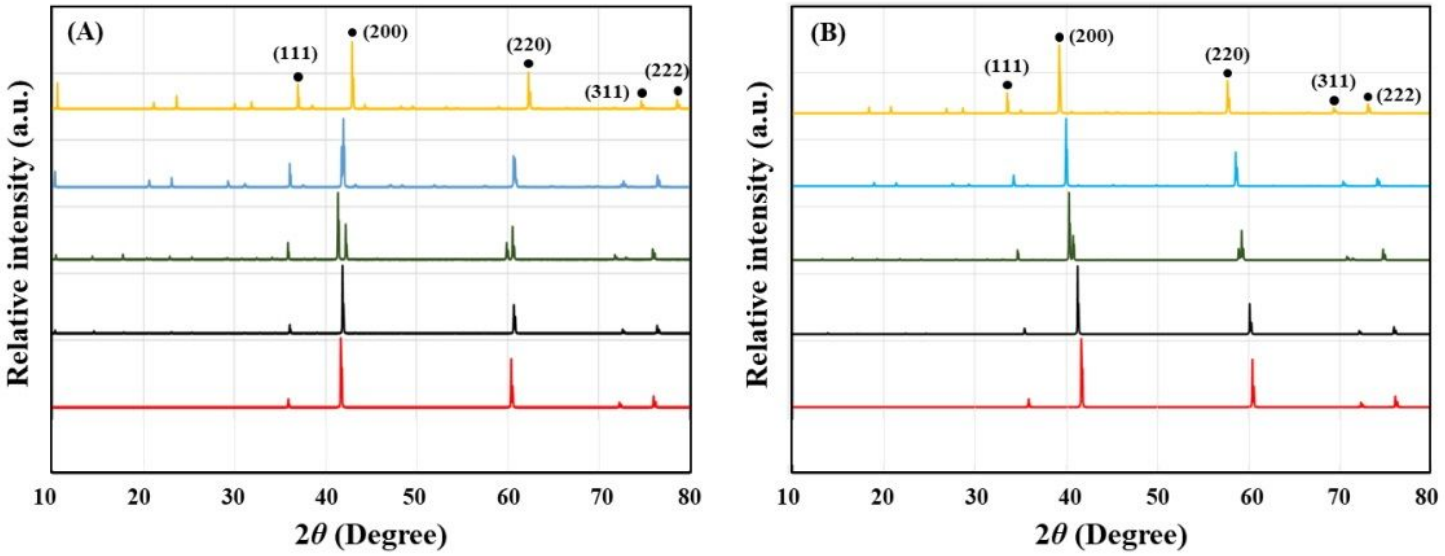

Figure 10

XRD results obtained from simulation for MgO-based binary powders: (A) Mg1−xNixO and (B) Mg1−xMnxO. The red, black, green, blue, and yellow patterns in each figure indicate MgO, Mg0.985M0.015O, Mg0.97M0.03O, Mg0.94M0.06O, and Mg0.88M0.12O, respectively.

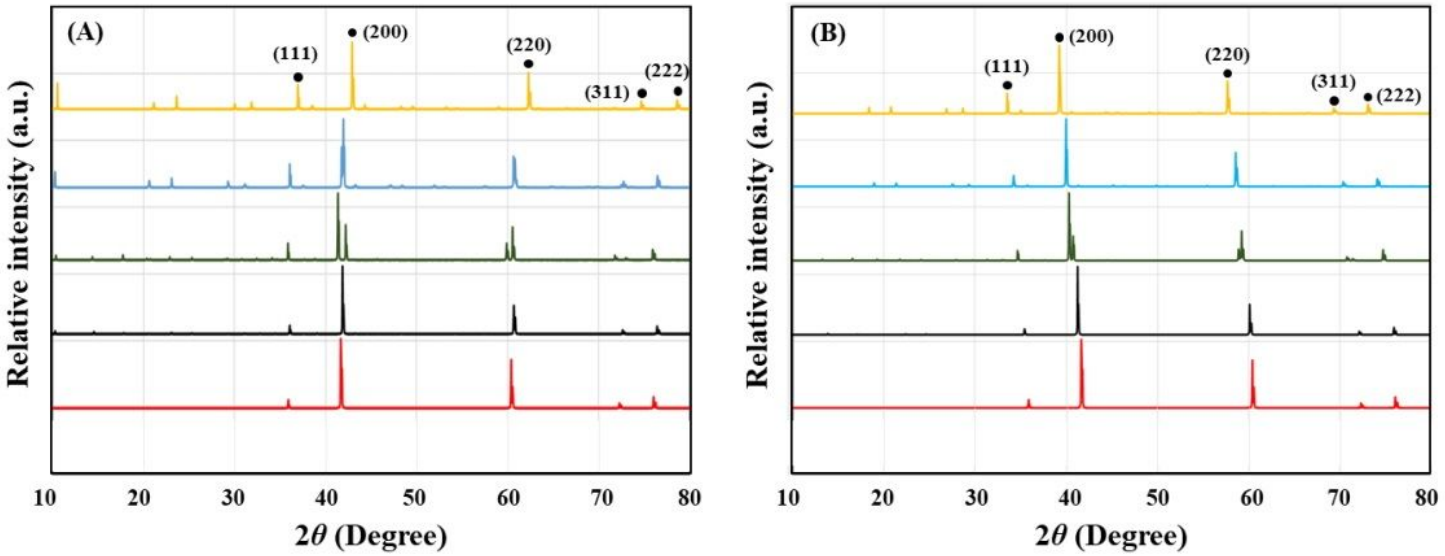

Figure 10

XRD results obtained from simulation for MgO-based binary powders: (A) Mg1−xNixO and (B) Mg1−xMnxO. The red, black, green, blue, and yellow patterns in each figure indicate MgO, Mg0.985M0.015O,

Mg0.97M0.03O, Mg0.94M0.06O, and Mg0.88M0.12O, respectively.

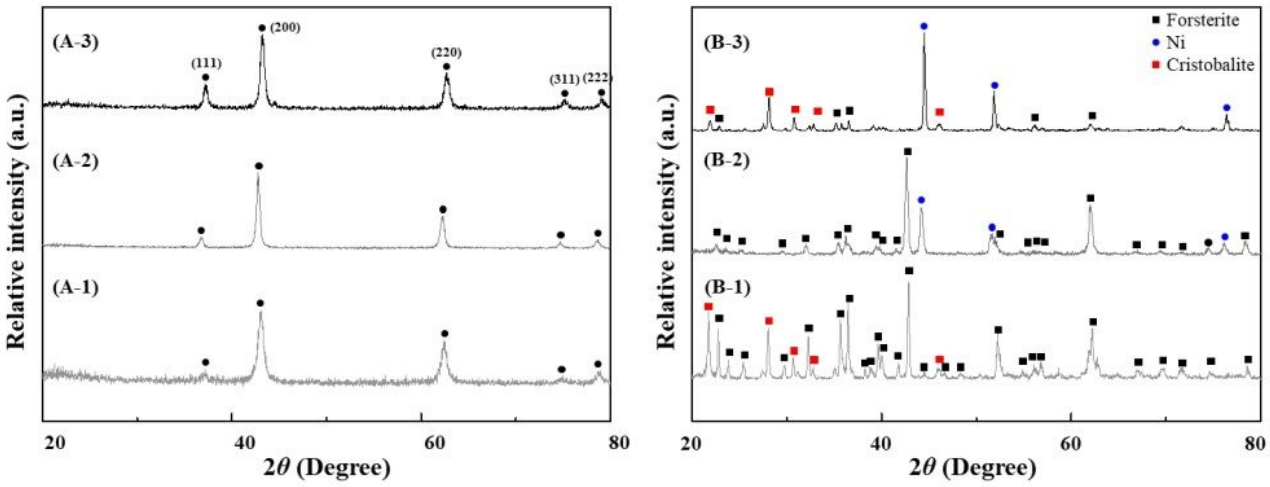

Figure 11

XRD results before and after the reaction between Mg1−xNixO and SiO2: (A) before reaction and (B) after reaction. Each number indicates MgO + SiO2, Mg0.9Ni0.1O + SiO2, and Mg0.7Ni0.3O + SiO2.

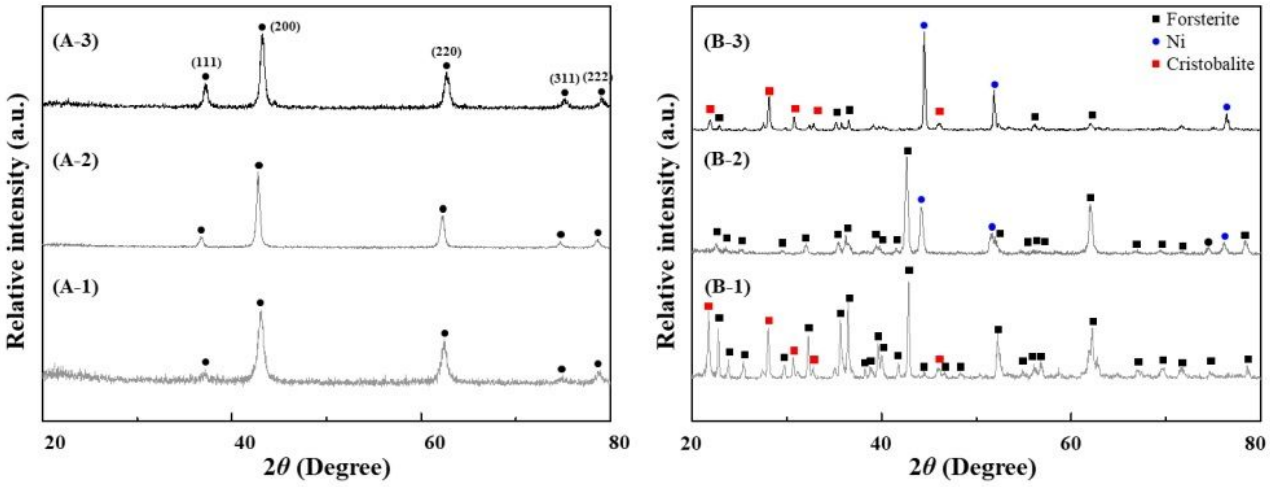

Figure 11

XRD results before and after the reaction between Mg1−xNixO and SiO2: (A) before reaction and (B) after reaction. Each number indicates MgO + SiO2, Mg0.9Ni0.1O + SiO2, and Mg0.7Ni0.3O + SiO2.

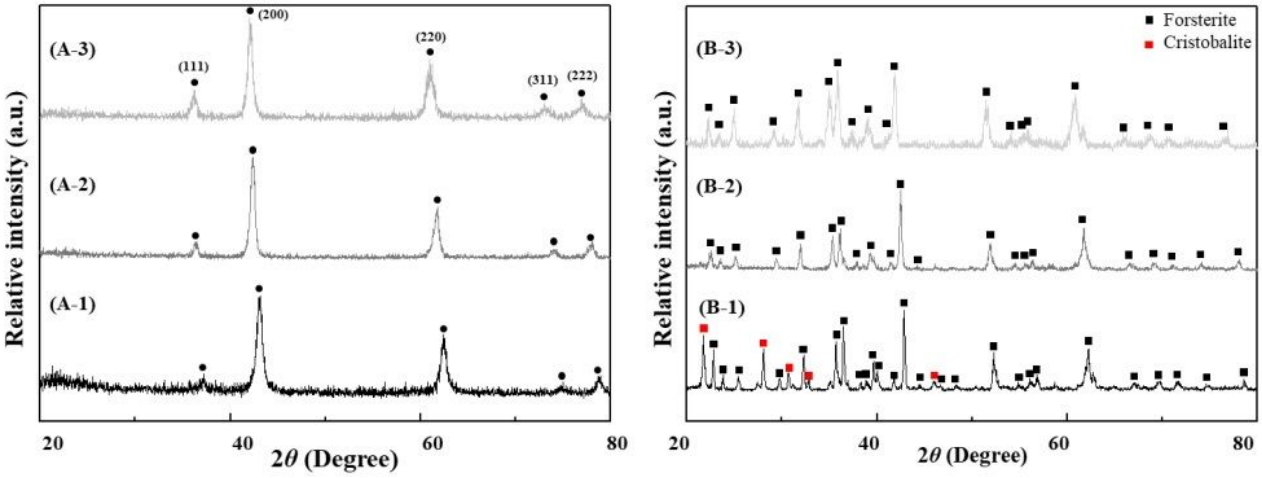

Figure 12

XRD results before and after the reaction between Mg1−xMnxO and SiO2: (A) before reaction and (B) after reaction. Each number indicates MgO + SiO2, Mg0.9Mn0.1O + SiO2, and Mg0.7Mn0.3O + SiO2.

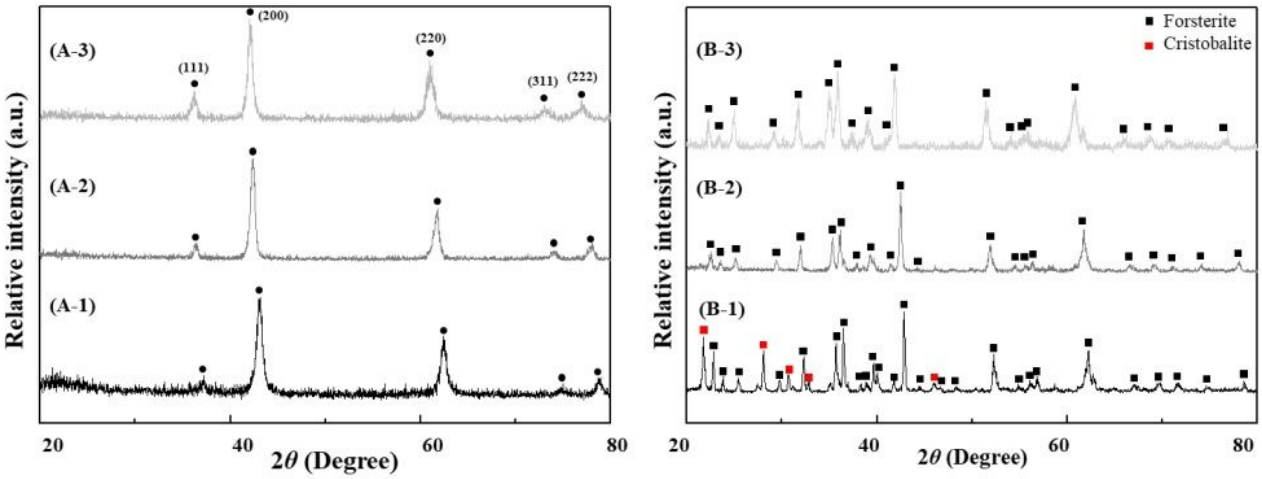

Figure 12

XRD results before and after the reaction between Mg1−xMnxO and SiO2: (A) before reaction and (B) after reaction. Each number indicates MgO + SiO2, Mg0.9Mn0.1O + SiO2, and Mg0.7Mn0.3O + SiO2.

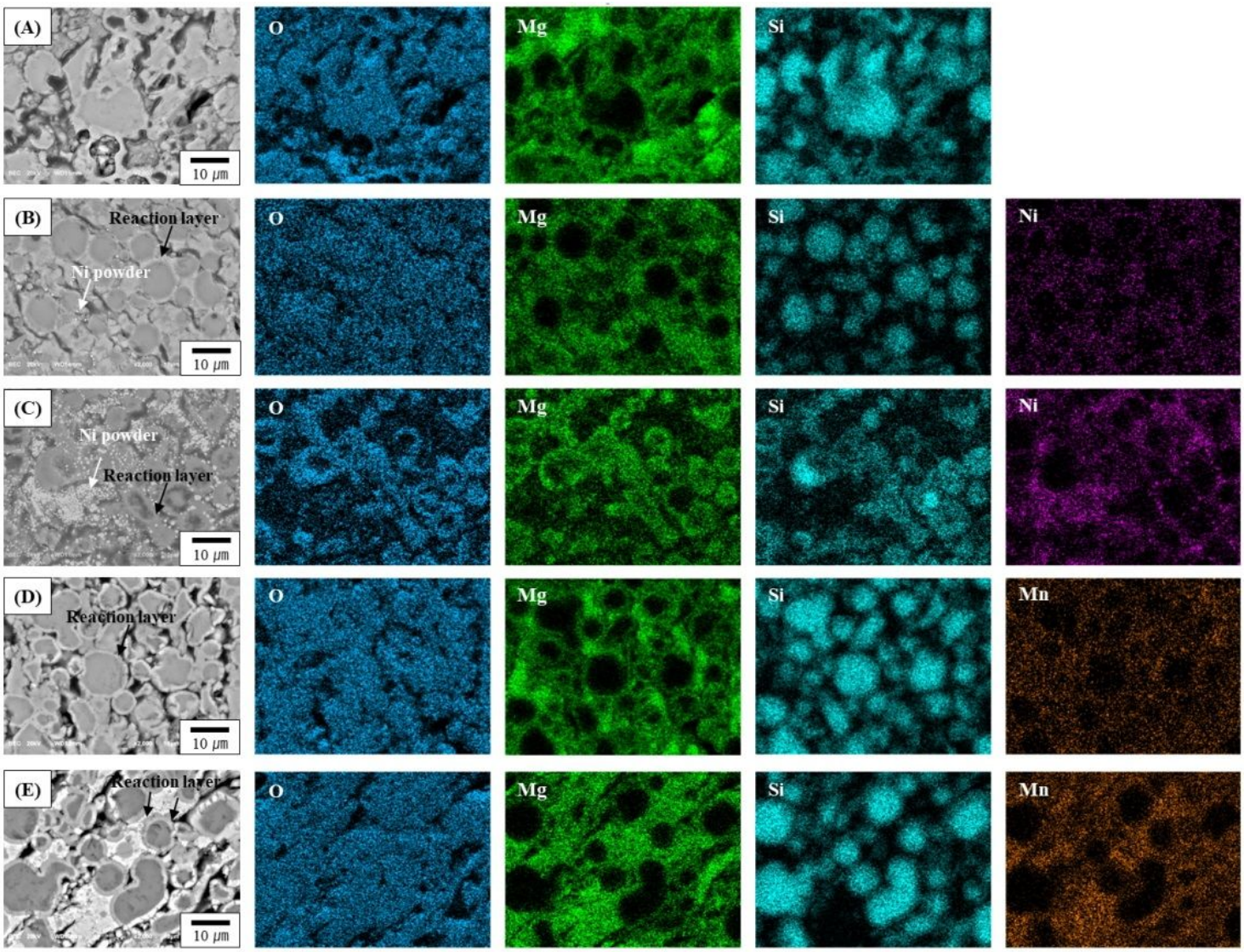

Figure 13

Microstructure and element analysis after the reaction between Mg1−xMxO powders and SiO2: (A) MgO + SiO2, (B) Mg0.9Ni0.1O + SiO2, (C) Mg0.7Ni0.3O + SiO2, (D) Mg0.9Mn0.1O + SiO2, and (E) Mg0.7Mn0.3O + SiO2.

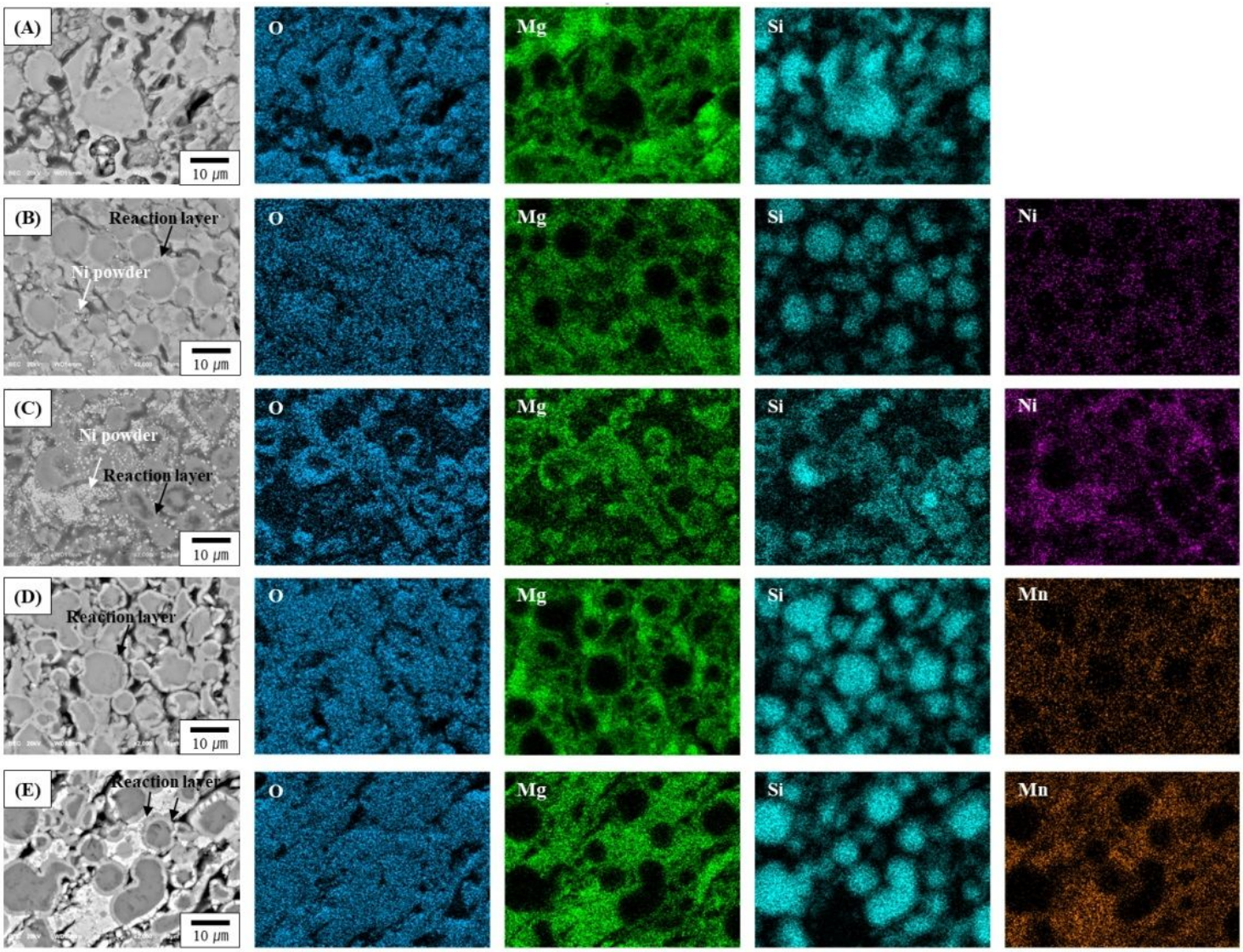

Figure 13

Microstructure and element analysis after the reaction between Mg1−xMxO powders and SiO2: (A) MgO + SiO2, (B) Mg0.9Ni0.1O + SiO2, (C) Mg0.7Ni0.3O + SiO2, (D) Mg0.9Mn0.1O + SiO2, and (E) Mg0.7Mn0.3O + SiO2.

Supplementary Files

This is a list of supplementary files associated with this preprint. Click to download.

- Tableforsubmission.docx
- Tableforsubmission.docx